WNKs regulate mouse behavior and alter central nervous system glucose uptake and insulin signaling

Ankita B. Jaykumar [1+], Derk Binns [1], Clinton A. Taylor IV [1], Anthony Anselmo [1#], Shari G. Birnbaum[2], Kimberly M. Huber[3], Melanie H. Cobb [1]

From the Departments of [1]Pharmacology, UT Southwestern Medical Center, Dallas, USA, [2]Peter O'Donnell Jr. Brain Institute and Psychiatry, UT Southwestern Medical Center, Dallas, USA. [3]Department of Neuroscience, UT Southwestern Medical Center, Dallas.

*Corresponding author: Melanie.Cobb@UTSouthwestern.edu
[+]Co-corresponding author: Ankita.Jaykumar@UTSouthwestern.edu

6001 Forest Park Rd., Dallas, Texas 75390-9041; Tel. 214 645-6122; Fax 214 645-6124

#Current affiliation: Dana-Farber Cancer Institute, Center for Cancer Genomics, Boston, MA-02115, USA.

Key words: WNK, insulin signaling, neuronal glucose metabolism, sortilin, TBC1D4/AS160, anxiety, memory, GLUT4 trafficking

Abstract

Certain areas of the brain involved in episodic memory and behavior, such as the hippocampus, express high levels of insulin receptors and glucose transporter-4 (GLUT4) and are responsive to insulin. Insulin and neuronal glucose metabolism improve cognitive functions and regulate mood in humans. Insulin-dependent GLUT4 trafficking has been extensively studied in muscle and adipose tissue, but little work has demonstrated either how it is controlled in insulin-responsive brain regions or its mechanistic connection to cognitive functions. In this study, we demonstrate that inhibition of WNK (With-No-lysine (K)) kinases improves learning and memory in mice. Neuronal inhibition of WNK enhances *in vivo* hippocampal glucose uptake. Inhibition of WNK enhances insulin signaling output and insulin-dependent GLUT4 trafficking to the plasma membrane in mice primary neuronal cultures and hippocampal slices. Therefore, we propose that the extent of neuronal WNK kinase activity has an important influence on learning, memory and anxiety-related behaviors, in part, by modulation of neuronal insulin signaling.

Background

Traditionally, the brain was considered an insulin-insensitive organ, based on whole-brain glucose uptake studies [1,2]. In contrast, more recent work has identified discrete areas of the brain, notably the hippocampus, cortex and the amygdala, that express high levels of insulin receptors and the insulin-sensitive glucose transporter glucose transporter-4 (GLUT4) [3-8]. In muscle and adipose tissue, insulin activates phosphatidylinositol 3-kinase (PI3K) and AKT (aka protein kinase B) signaling to cause the hallmark action of insulin in these tissues to increase GLUT4 translocation to the plasma membrane to facilitate insulin-dependent glucose uptake [9-10]. In a similar way, increases in neuronal insulin concentration also promote GLUT4 membrane translocation *via* PI3K/AKT signaling in neuronal cells [11-20]. Neuronal insulin signaling improves learning, memory and mood in humans and in animal models [18-29]. Glucose utilization increases in the hippocampus during memory tasks; performance on these challenging tasks is critically determined by an adequate supply of glucose to this brain region [30-42]. Recent studies show that hippocampal GLUT4 translocates to the plasma membrane during memory training. Further, acute intrahippocampal inhibition of GLUT4-mediated glucose transport impairs memory acquisition [18-19]. In addition, disrupted glucose metabolism in the hippocampus and other regions is associated with anxiety disorders [27-28, 37-38, 43-72]. These findings lead to the supposition that memory is enhanced, at least in part, *via* local neuronal insulin-dependent upregulation of glucose uptake to increase glucose available for metabolism.

The four WNKs (With-No-lysine (K) 1-4) are serine/threonine protein kinases best known for regulation of ion transport. One or more family members are responsible for rare hereditary diseases including forms of hypertension and sensory neuropathy [73-75]. The best characterized WNK substrates are the closely related kinases with overlapping functions that belong to the STE branch of the kinome tree: OSR1 (*OXSR1*, Oxidative stress response kinase 1) and SPAK (*STK39*, STE20/SPS-1-related proline-alanine-rich kinase) [76]. WNKs bind, phosphorylate, and activate OSR1 and SPAK which in turn phosphorylate downstream targets including the cation-chloride co-transporters NKCC1/2 (*SLC12A1/2*, $Na^+/K^+/2Cl^-$ co-transporter), NCC (*SLC12A3*, $Na^+/2Cl^-$ co-transporter) and KCC2 (*SLC12A5*, $K^+/2Cl^-$ co-transporter) [76]. Genome-wide association studies have identified multiple SNPs in WNKs and several of these downstream effectors that are associated with impairment in learning, intellectual abilities, neuropsychiatric and age-related neurodegenerative diseases such as Alzheimer's Disease

(AD) etc. [77-94]. Abnormal activities of WNKs and their downstream effectors are also associated with these traits [95-109].

WNKs also regulate trafficking of many membrane transporters and ion channels [73, 110-119]. In addition to these well-characterized roles of WNKs, several studies have also suggested connected actions between WNK1 and AKT in cell lines and in kidneys including in hyperinsulinemic db/db mice [120-130]. PI3K/AKT signaling has been implicated in the regulation of memory and anxiety in mice [37,38]. These and other findings led us to hypothesize a critical function of the WNK pathway in memory and anxiety *via* regulating multiple steps in vesicle trafficking to modulate insulin-responsive GLUT4 translocation in neurons.

Results

Inhibition of hippocampal WNK in mice enhances learning and memory. WNK and its downstream signaling mediators (**Figure 1A**) have been associated with learning and memory in animal models [77-90, 95-109]. To examine the potential of WNKs on mouse learning and memory performance, we used the orally bioavailable pan-WNK inhibitor WNK463: this compound is selective for WNKs over other enzymes based on a library of >400 protein kinases [131]. First, we evaluated the effectiveness of oral administration of WNK463 to inhibit WNKs in the mouse hippocampus. Phosphorylation of the WNK substrate OSR1 was a readout of WNK activity. Using this method, WNK463 decreased pOSR1 (**Figure 1B**) but had no adverse effect on mouse body weight (**Figure S1A**). We then tested the effect of WNK inhibition on memory performance by the Novel Object Recognition test. The Novel Object Recognition test takes advantage of the natural proclivity of mice to explore novelty; if a mouse recognizes a familiar object, it will spend more time exploring a novel object (**Figure 1C**). Therefore, longer time spent exploring a novel object compared to a familiar object (ie: a higher discrimination index [see methods for details]) is suggestive of better learning and/or memory. We found that the discrimination index for mice treated with oral WNK463 was significantly higher than that for vehicle-treated mice (**Figure 1D**), while the total exploration time during the test was similar between both groups (**Figure S2A**). This suggests that inhibition of WNK in mice *via* WNK463 leads to enhanced learning and memory. We further tested the effect of WNK inhibition on hippocampal-dependent memory using the Contextual Fear Conditioning Test (**Figure 1E**). In this test, WNK463-treated mice froze significantly longer than vehicle-treated mice during the context test, indicative of enhanced contextual memory in WNK463-treated mice (**Figure 1F**). However, no significant difference in freezing time was observed between the groups in the cue

test, which assesses function of the amygdala, a major processing center of the brain for emotions such as fear (**Figure 1G**). To determine whether the increased freezing behavior might be due to an adverse effect of the drug or a confounding factor such as lethargy, we performed a locomotor test in a home cage-like environment (**Figure 1H**). We found no differences in their locomotor activity, making adverse effects unlikely to account for the results of the freezing test (**Figure 1I**). Results of these tests are consistent with the interpretation that WNK inhibition enhances learning and memory (**Figure 1J**).

Inhibition of hippocampal WNK enhances anxiety-related behavior in mice. While the hippocampus is critical for cognitive processes such as episodic memory and spatial navigation, it is also implicated in the pathogenesis of anxiety disorders [18-28]. Several studies have confirmed a close correlation between anxiety and emotional memory [27-28, 37-38]. Enhanced fear-based contextual memory in WNK463-treated mice prompted us to test whether anxiety-like behaviors are altered in these mice. We found no difference in basal anxiety measured by the Open-Field test (**Figure 2A, 2B, 2C**) or the Elevated Plus Maze test (**Figure 2D, 2E, 2F**), between the vehicle and the WNK463-treated groups. However, stressing WNK463-treated mice with electric foot-shocks prior to the anxiety tests results in higher measures of anxiety. Mice treated with oral WNK463 spent less time in the center of the Open-Field test chamber relative to control mice, indicative of a higher level of anxiety (**Figure 2G, 2H**). Similarly, these mice spent less time in the open arm of the Elevated Plus Maze compared to the control mice, also indicative of higher anxiety levels (**Figure 2I, 2J**). Yet, the total distance moved by mice during both of these tests was not different between the groups (**Figure S3A, S3B, S3C, S3D**). This suggests that WNK463 only enhanced anxiety in mice pre-exposed to trauma such as electric foot-shocks.

Inhibition of WNK augments glucose uptake via GLUT4. Insulin action and glucose uptake into select regions of the brain are thought to regulate memory and anxiety-like behavior in mice [18-32, 37-38, 43-72] (**Figure 3A**). Because WNK inhibition enhanced memory performance and anxiety in mice, we tested whether inhibition of WNKs in insulin-sensitive areas of the brain enhanced 2-deoxyglucose uptake using an *in vivo* radioactive 2-deoxy glucose uptake assay in mice. Dissecting the hippocampi of mice treated with WNK463, we found 2-deoxyglucose uptake in this insulin-sensitive region was elevated compared to hippocampi from mice treated with vehicle (**Figure 3B**). These data together suggested that inhibition of hippocampal WNK enhanced *in vivo* hippocampal glucose uptake in mice. Next, we cultured hippocampal slices from mouse brain, and found that inhibition of WNK enhanced 2-deoxyglucose uptake in these

hippocampal slice cultures (**Figure 3C**). We also isolated crude synaptosomes from mouse brain and found that inhibition of WNK enhanced 2-deoxyglucose uptake in these synaptosomes (**Figure 3D**). To examine the effect of insulin in cultured cells, SH-SY5Y cells were differentiated to neuronal-like cells *in vitro* [132]. Stimulation of these cells with insulin induced [^{3}H]-2-deoxyglucose uptake that was further enhanced by simultaneous inhibition of WNKs. In addition, WNK463 alone enhanced 2-deoxyglucose uptake compared to DMSO control (**Figure 3E**).

Because insulin regulates GLUT4, we asked whether increased glucose uptake in WNK-inhibited neuronal cells depends on GLUT4 [70-72]. Differentiated SH-SY5Y cells were treated with indinavir, a GLUT4 inhibitor, to identify the contribution of GLUT4 to enhanced uptake caused by WNK463. Indinavir reduced the enhanced insulin-stimulated 2-deoxyglucose uptake observed with WNK inhibition, suggesting a role for GLUT4 in facilitating at least a fraction of glucose uptake responsive to WNK blockade (**Figure 3F**). To obtain further evidence for the involvement of GLUT4, we examined GLUT4 localization in mice hippocampal slices using surface biotinylation. WNK inhibition with WNK463 enhanced insulin-stimulated GLUT4 surface expression relative to insulin alone (**Figure 3G, 3H**). We obtained similar results using differentiated SH-SY5Y cells for surface biotinylation in the presence of WNK463, insulin or both (**Figure S4A, S4B**). Together, these data suggest that inhibition of WNK in neuronal cells enhances insulin-dependent glucose uptake via enhanced GLUT4 surface targeting.

Inhibition of WNK enhances AKT signaling in the hippocampus and cell culture. Insulin induces activation of PI3K/AKT signaling to cause GLUT4 translocation to the plasma membrane to facilitate insulin-dependent glucose uptake [9-10] (**Figure 4A**). Given the involvement of insulin in regulating GLUT4 trafficking, we asked whether inhibition of WNK in neuronal cells affects insulin signaling to PI3K/AKT. Multiple groups including ours have previously reported inhibitory cross talk between WNK1 and AKT [120-130]. In homogenates of excised hippocampal tissue from mice treated with oral WNK463 compared to vehicle, we found enhanced phosphorylation of AKT (pAKT- at Ser473 which is an activating phosphorylation site on AKT) (**Figure 4B**), indicative of enhanced insulin signaling. In differentiated SH-SY5Y neuroblastoma cells, we found that co-treatment with insulin and the WNK inhibitor enhanced pAKT compared to insulin alone (**Figure 4C, 4D**). This is consistent with enhanced insulin signaling resulting from WNK inhibition. In dissociated mouse primary neuronal cell culture, we found that WNK inhibition enhanced pAKT compared to vehicle control (**Figure 4E, 4F**),

although in this case, WNK inhibition and insulin co-treatment failed to further enhance activation of AKT compared to insulin alone.

OSR1/SPAK interact with molecular mediators of GLUT4 trafficking. Upon insulin signaling, AKT phosphorylates the AKT-substrate of 160-kDa (AS160, *TBC1D4*) [116-118], a Rab GTPase-activating protein critical in liberating the static pool of GLUT4 from its storage vesicle site to promote its exocytosis [117-118]. Studies conducted by the Jordan lab suggested that WNK1 regulates surface trafficking of the constitutive glucose transporter GLUT1 by binding AS160 and subsequently identified WNK1 phosphorylation sites in the protein [116-117]. OSR1 and SPAK are two-domain enzymes containing a kinase domain and a conserved carboxy-terminal (CCT) domain that houses a docking site for proteins containing short basic/hydrophobic motifs, subsequently confirmed through structural analysis [76]. Protein interaction studies showed that the motif, most typically R-F-x-V/I or R-x-F-x-V/I often forms the basis for substrate recognition [110,133]. Bioinformatic analysis of motif interactions with the CCT, returned AS160 as a likely OSR1/SPAK binding protein through its R-x-F-x-I motif [134]. Thus, we asked whether the WNK/OSR1/SPAK pathway regulates GLUT4 trafficking [119], in part by modulating AS160 function (**Figure 5A**). First, we found that endogenous AS160 from mouse brain lysates co-immunoprecipitated with OSR1 (**Figure 5B**). To ask whether the interaction between AS160 and OSR1 is modulated by insulin, we immunoprecipitated endogenous AS160 from differentiated SH-SY5Y cells treated with or without insulin and quantified the amount of OSR1 that co-immunoprecipitated. We found that insulin treatment enhanced the interaction between AS160 and OSR1, suggesting that insulin influences the OSR1-dependent effect on AS160 localization. We also found that co-treatment with WNK463 reduced the interaction between AS160 and OSR1 (**Figure 5C, 5D**). Insulin regulates AKT-dependent phosphorylation of AS160 on Ser588. We found enhanced phosphorylation of Ser588 on AS160 following WNK inhibition consistent with the increase in AKT activity caused by suppressing WNK activity (**Figure 5E, 5F**).

Using an *in vitro* pull-down assay with purified SPAK isolated from Human Embryonic Kidney (HEK293T) cells, 3xFlag-SPAK (residues 50-545), co-immunoprecipitated with an overexpressed fragment of AS160 (residues 193-437) containing the R-x-F-x-V motif. Moreover, this interaction was diminished by co-incubation with a blocking peptide derived from WNK1 (SAGRRFIVSPVPE; residues 1253-1265) that competes for docking interactions on the OSR1/SPAK CCT domain (**Figure 5G, 5H**). This suggests that AS160 associates with SPAK during insulin signaling. Thus, the WNK/OSR1/SPAK pathway communicates with this step of

the GLUT4 translocation process via direct interaction of AS160 with OSR1/SPAK and through enhancing AKT activity to phosphorylate AS160. These data reveal the potential of WNK/OSR1/SPAK to influence insulin-sensitive GLUT4 trafficking at this essential step of the process.

Optimal GLUT4 trafficking to the membrane in response to insulin treatment is contingent on its efficient sequestration in specialized GLUT4 storage vesicles, a phenomenon common to both neurons and peripheral insulin-sensitive tissues [9-11]. The protein sortilin (*SORT1*, also known as Neurotensin receptor-3) is essential for the formation of and, retrieval of GLUT4 to these static storage vesicles in the trans-Golgi network (TGN) which allows efficient GLUT4 translocation to the plasma membrane upon insulin treatment [11,135-139]. Sortilin-mediated GLUT4 retrograde trafficking and sequestration is critically dependent on a highly conserved motif with the consensus R-F_{787}-L-V in sortilin [70-71,140]. However, the underlying molecular mediators that regulate this crucial process are unknown. Our motif bioinformatics also predicted that the R-F-x-V motif in the C-terminus of sortilin binds to the OSR1/SPAK CCT domain and raised the possibility that this plays a critical role in regulating retrograde trafficking of GLUT4 to the TGN [110,133]. Therefore, we asked whether WNK/OSR1/SPAK interacts with sortilin. We found that OSR1 and sortilin colocalize in differentiated SH-SY5Y cells (**Figure 5I**). We also found that endogenous OSR1 and sortilin co-immunoprecipitate from differentiated SH-SY5Y cells (**Figure 5J**). Previously, a yeast-two-hybrid screen using the OSR1 CCT domain as bait had returned sortilin as a potential binding partner (**Figure 5K**). To determine whether or not the interaction between the CCT domain of OSR1 and sortilin is facilitated by its R-F-x-V motif, we overexpressed sortilin in HEK293 cells and immunoprecipitated it. We found that OSR1 was also recovered in the sortilin precipitate. Co-immunoprecipitation of OSR1 with sortilin is prevented by co-incubation with the blocking peptide that competes with the R-F-x-V docking motif for binding to the OSR1 CCT (**Figure 5L, 5M**). As a further confirmation, we tested the binding affinities of wild-type sortilin and sortilin R-F-x-V motif mutant peptides with bacterially expressed purified His_6-SPAK CCT domain (residues 433-527). We found that only the WT sortilin peptide bound strongly to the CCT domain, while substitution of the motif R with K or A led to a drastic reduction in binding affinity. This implies that the interaction between sortilin and OSR1/SPAK CCT domain is facilitated via the key sortilin R-F-x-V motif (**Figure S5A**). These findings lead to the idea that WNK impacts this essential step in GLUT4 trafficking through binding of its effector kinases OSR1/SPAK to sortilin. Together, our results suggest that WNK/OSR1/SPAK influences insulin-sensitive GLUT4 trafficking by balancing GLUT4

sequestration in the TGN via regulation of sortilin with GLUT4 release from these vesicles upon insulin stimulation via regulation of AS160 (**Figure 5A**).

Discussion

Insulin sensitivity is highly dependent upon confinement of GLUT4 in specialized GLUT4 storage vesicles until insulin signals a release from these vesicles to promote GLUT4 membrane translocation [9-11]. In insulin-resistant states, derangements in the formation and retention of GLUT4 in these static vesicles, impairs insulin-responsive GLUT4 translocation [72]. In peripheral tissues, insulin resistance is associated, in part, with reduced glucose transport due to a loss-of-function in insulin-regulated GLUT4 [63]. Underlying mechanisms in the brain, however, remain unclear. Here we evaluated two proteins, sortilin and AS160, important for GLUT4 trafficking. Sortilin which is widely expressed in neurons is suggested to be a critical mediator of this process and hence an important determinant of neuronal insulin sensitivity [11,135-139,141]. AS160 is phosphorylated by AKT upon insulin stimulation and causes the release of GLUT4 trapped in the static GLUT4 storage vesicles leading to exocytosis and surface delivery of GLUT4 to promote glucose uptake into cells [118]. In this study, we demonstrate actions of the WNK pathway on these two GLUT4 trafficking mediators sortilin and AS160. Our study shows that WNKs can affect both capture of GLUT4 in storage vesicles via sortilin as well as the release of trapped GLUT4 from the storage vesicles to facilitate glucose uptake into the cells via AS160. This work reveals at least two sites of action of the WNK pathway on a hallmark action of insulin- translocation of GLUT4 to the plasma membrane.

We suggest that the downstream effector kinases OSR1/SPAK have positive and perhaps required actions in this pathway. OSR1 appears to be needed for proper sequestration of GLUT4 in, and possibly release of GLUT4 from the storage vesicles. As a result, overall, the WNK pathway appears to be a positive regulator of GLUT4 trafficking. This is consistent with results of two other studies from different laboratories. The first study in skeletal muscle shows that loss of WNK1 (*rather than inhibition of activity*) drastically reduced GLUT4 localization to the plasma membrane in response to insulin, suggesting that WNK is essential for this trafficking event [119]. The second study shows that overexpression of the C-terminal tail of sortilin containing the R-F-x-V motif had an inhibitory effect on GLUT4 trafficking [142], suggesting that blocking the action of OSR1/SPAK prevents proper GLUT4 sequestration in storage vesicles. We anticipate that in the absence of a stimulus or a WNK inhibitor, low level WNK activity is sufficient to support OSR1/SPAK function to permit some of the trafficking functions of these proteins, including aiding the basal function of sortilin and GLUT4 assembly in

storage vesicles, which may also involve AKT [142]. Then, activation of AKT by insulin will release GLUT4 to the membrane, independent of a substantial change in WNK activity. If this were not the case, only in cells in which WNK1 was highly active, could OSR1 function as a component of the sequestration step or the transfer mechanism mediated by AS160 as a result of insulin-stimulated AS160-OSR1 binding. Chemical inhibition of WNK1 will enhance AKT to increase its transporter localization to the plasma membrane. However, under normal conditions, in the absence of an inhibitor, basal/low level WNK activity will be adequate to permit the sortilin get-ready steps in vesicle formation and insulin/AKT will do the rest. We are working to establish the validity of this proposed explanation.

In addition to results presented here with WNK inhibition, several lines of evidence suggest cross-talk among AKT and WNK1 signaling pathways [120-130]. One early study suggested that insulin induces phosphorylation of the WNK downstream target, NCC ($Na^+/2Cl^-$ cotransporter) in mouse kidney cells [123]. WNK1 is a substrate of AKT which phosphorylates it on Thr60 [124-125] but phosphorylation on this residue has not been shown to affect WNK catalytic activity, although several studies have used WNK1 pThr60 as a proxy for its function [119, 143]. In mouse embryonic fibroblasts it was reported that phosphorylation of WNK1 T60 by AKT promotes its degradation via the ubiquitin-proteasome pathway [129]. Phosphorylation of WNK1 on T60 contributes to the activation of the Serum and Glucocorticoid Regulated kinase 1 (SGK1) in a PI3K-dependent manner [127-128]. WNK1/SGK1 signaling is chronically activated in the AKT3 knockout mice model, contributing to high fat diet-induced metabolic syndrome, and this was reversed upon SGK1 inhibition [129-130]. The PI3K/AKT pathway activates the WNK-OSR1/SPAK/NCC cascade in hyperinsulinemic db/db mouse, model of insulin resistance [122]. In contrast, another study reported diminished insulin/AKT/WNK1 functions in diabetic skeletal muscle [119]. Although mechanistic clarity is lacking, together these findings suggest a critical role of aberrant WNK1 signaling in the development of metabolic syndrome. In this study, we show that WNK inhibition using the inhibitor WNK463 enhances insulin/AKT signaling, suggesting a reciprocal cross-talk between WNK pathway and insulin/AKT signaling. Interestingly, db/db mice exhibit progressive age-dependent decrease in AKT activity, surface GLUT4 as well as dysregulated WNK signaling in the hippocampus and this impairment occurs prior to the overt development of cognitive decline in this mouse model [66-69,144-154]. Interventions that correct dysregulated AKT downstream function ameliorated cognitive impairment in db/db mice [151,155,156]. Thus, we propose that aberrant WNK signaling can impact cognitive decline due to insulin/AKT metabolic dysregulation.

Sortilin is a member of the family of vacuolar protein sorting 10 protein (VPS10P) domain receptors. In addition to its glucose transport function, it has multiple actions in neurons [157-159]. Genetic and functional studies implicate sortilin and sortilin-related receptor 1 in aging, age-related cognitive decline, and AD [157-164]. Mechanistically, sortilin is involved in trafficking of BDNF, implicated in memory processes [158]. It also mediates endocytic uptake of Apolipoprotein E (APOE)-bound amyloid-β-containing lipoproteins in neurons [159]. The APOE-(4) isoform of APOE bears significance as the major genetic risk factor for late-onset AD [165-168]. Functionally, the APOE4 isoform perturbs sortilin trafficking [93] and impairs neuronal insulin signaling by disrupting insulin receptor trafficking [169]. Humans carrying the APOE4 isoform exhibit compromised glucose metabolism and downregulation of GLUT4 expression in the hippocampus, probably via affecting sortilin trafficking [170]. Our study suggests that inhibition of WNK kinases promotes glucose uptake in mice hippocampi and regulate hippocampus-dependent memory. Mechanistically, this could be, in part, due to regulation of sortilin.

Many studies have linked abnormal WNK activity to an array of neurological diseases. Several SNPs, mutations and aberrant activities in WNK pathway components have been associated with learning disabilities, neuropsychiatric and neurodegenerative diseases [77-109,91-94]. WNK1 is highly expressed in the CA1-CA3 regions of the dorsal hippocampus, implicated in contextual memory [171]. WNK1 is differentially expressed in the hippocampus from schizophrenic and AD patients [101-102]. Several pathogenic variants in the *WNK3* gene cause intellectual disability [94]. Several mutations in the *WNK3* gene were identified in schizophrenic patients and expression of WNK3 protein was also elevated in these patients [99,103,172]. WNK3 regulates the splicing factor Fox-1 implicated in anxiety disorder and schizophrenia [107,173]. Activities of some well-characterized downstream effectors of the WNK pathway, e.g., OSR1, SPAK, NKCC1 and KCC2, are altered in the hippocampus in multiple models of neuropsychiatric diseases and neurodegenerative diseases [95-106]. The control of ion homeostasis has been assumed to be the mechanism underlying the above-mentioned neuro-pathophysiologies. Our study adds insights on the possible underlying causes of WNK pathways in regulating neuronal functions.

Aging is a major risk factor for the development of diabetes and severe insulin resistance [174,175]. Neuronal insulin resistance marked by striking reductions in insulin signaling and disrupted hippocampal glucose uptake are early indicators of cognitive decline in age-related diseases such as Alzheimer's Disease (AD) [43-62]. Interestingly, the neurocognitive

impairment commonly known as HIV-associated neurocognitive disorder is prevalent in HIV patients administered anti-retroviral GLUT4-impairing protease inhibitors (indinavir, nelfinavir) compared to patients treated with GLUT4-sparing protease inhibitors (such as Atazanavir) [64-65]. Animal models of insulin resistance exhibit diminished hippocampal plasma membrane GLUT4 [63-67] and correction of insulin resistance rescued the impairment in hippocampal-dependent memory and synaptic plasticity [68-69]. Therefore, several lines of research converge to suggest that aberrant insulin-responsive GLUT4 translocation causes hippocampal cognitive dysfunction, an overlap between metabolic and cognitive disorders. Our study suggests that WNK kinases are critical mediators of insulin sensitivity in neurons which affects learning and memory. Aberrant regulation of these kinases could disrupt normal neuronal behavior. Therefore, an important direction for future studies will be to determine how WNK regulates cognitive behavior in neuronal insulin resistant states.

Methods

Cell lines. The human neuroblastoma cell line (SH-SY5Y: ATCC, CRL-2266) was grown in low glucose DMEM medium (11885084, Thermo Fisher Scientific) with 10% fetal bovine serum (Sigma-Aldrich, F0926), 1% L-glutamine, 1% penicillin and streptomycin. SH-SY5Y cells were differentiated in Neurobasal medium (21-103-049, Fisher Scientific) with Glutamax^{TM} (35-050-061, Fisher Scientific), B27 supplement (17504044, Thermo Scientific), 1% penicillin and streptomycin along with 10 μM retinoic acid (R2625, Millipore Sigma) [132]. Alternatively, for glucose uptake assays, these cells were differentiated in low glucose DMEM (Thermo Fisher Scientific, 11885084) with 10 μM retinoic acid. Human embryonic kidney cells (HEK293) were purchased from ATCC (CRL-1573) and were grown in DMEM medium with 10% FBS and 1% penicillin-streptomycin. All the cells were maintained at 37°C and 5% CO_2.

Dissociated mouse primary cortical and glial cell culture. Dissociated cortical cultures were prepared from P0 mice using modified, previously published protocols [176]. Briefly, dissected cortex from P0 mice were trypsinized for 10min then dissociated by trituration. After centrifugation, neurons were plated in Neurobasal A medium (Invitrogen) containing B27 (2%; Invitrogen), 0.5 mM Glutamax, 1% Pen-Strep, and 5% fetal bovine serum (FBS) at a density of $8x10^5$ neurons per well of a 12-well dish each coated with 1 mg/ml poly-L-lysine overnight. Day 2, the medium was changed to Neurobasal A medium (Invitrogen), B27 (2%; Invitrogen), 0.5 mM Glutamax, without FBS. Day 3, cytosine arabinoside (1 μM) was added. Day 5, plates were washed 1 × with Neurobasal A with B-27 (Life Technologies) and 0.5 mM Glutamax and replaced with glial conditioned Neurobasal A medium containing B27, glutamine and cytosine

arabinoside (1 μM). Cultures were fed every 5 days by replacing 50% of the medium with glial conditioned medium. At day 21, neurons were treated as described.

Glial cultures were prepared from the neocortex of P0-P2 mouse pups and maintained in Neurobasal A containing 10% FBS, 2% B27 supplement and 50 μg/ml penicillin, 50 U/ml streptomycin, Sigma). Medium was replaced twice a week for 2-3 weeks. Cells were conditioned in Neurobasal medium lacking B27 and FBS for 48hr, collected and stored at 4°C for no more than one week prior to addition to neuronal cultures.

Hippocampal slices. Hippocampal slices (400 μm) were prepared from 30-45-day-old C57BL/6J mice as in [177]. Mice were anesthetized with xylaxine (4mg/ml)/ketamine (30 mg/ml). Mice were subjected to transcardial perfusion with ice-cold dissection buffer containing: 121 mM choline chloride, 2.5 mM KCl, 1.25 mM NaH_2PO_4, 5 mM dextrose, 30 mM $NaHCO_3$, 3 mM ascorbic acid and adjusted to 290 mOsm. Mice were decapitated, and the cerebrum was dissected from isolated brains and then sliced using a vibratome (VT 1000S; Leica, Nussloch, Germany) in the same ice-cold dissection buffer. The slices were transferred into a reservoir chamber filled with artificial cerebrospinal fluid (aCSF) containing 119 mM NaCl, 2.5 mM KCl, 31 mM $NaHCO_3$, 5 mM D-glucose, 1 mM NaH_2PO_4 [177]. Final concentrations of 1 mM $MgCl_2$ and 2 mM $CaCl_2$ were added just before use. Slices were allowed to recover for 2-3hr at 30°C. Both the aCSF and the dissection buffer were equilibrated with 95% O_2 and 5% CO_2.

Plasmid constructs. Sortilin full-length (NM_001205228) construct was cloned into a C-terminally tagged 3xFlag CMV14 vector (Sigma Aldrich) with restriction enzymes XbaI. Clones were screened by XbaI digests. Positive clones were verified by Sanger sequencing.

Yeast Two-Hybrid Analysis. A Jurkat T cell cDNA library (from Mike White, formerly Department of Cell Biology, University of Texas Southwestern Medical Center) was screened as described in [178]. Protein–protein interactions were tested by streaking co-transformants on medium lacking Leu, Trp, and His in addition to β-galactosidase assays.

Co-immunoprecipitation. Cells were lysed in lysis buffer (50mM HEPES, 150 mM NaCl, 5mM EDTA, 2% Triton X-100, 0.1% SDS) with 1:1000 protease inhibitor cocktail (stock containing: 583.2 μM pepstatin A, 762.4 μM leupeptin, 10.6 mM Nα-tosyl-L-arginine methyl ester HCl (Fisher Scientific, T03301G) , 10.8 mM tosyl-lysine-chloromethylketone HCl (Fisher Scientific, 50-397-132), 11.3 mM Nα-benzoyl-L-arginine methyl ester carbonate (Fisher Scientific, 50-501-393), 200 μM soybean trypsin inhibitor (Fisher Scientific, NC9065058)), 0.4 mM phenylmethylsulfonyl fluoride (PMSF) and phosphatase inhibitor- PhosStop (Sigma Aldrich, 4906837001). Cell extracts were harvested and cleared by centrifugation. Immunoprecipitation

(IP) buffer (50mM HEPES, 100 mM NaCl, 5mM EDTA, and 1% CHAPS (Sigma Aldrich, C3023) with protease inhibitor cocktail, PMSF and PhosStop (as above) was added in a 2:1 ratio to the cell lysate. Samples were incubated with primary antibody or rabbit IgG (control) for 3hr at 4°C and then with Protein A/G PLUS-Agarose (Santa Cruz Biotechnology, sc-2003) beads for 35min with head-to-tail rotation either in the absence or presence of 100 μM CCT blocking peptide SAGRRFIVSPVPE (United Biosystems). Samples were then washed three times with IP buffer before adding 6X SDS sample buffer (0.012% bromophenol blue, 30% glycerol, 10% SDS, 350 mM Tris-Cl, 5% β-mercaptoethanol) and heated at 90°C for 2min. Samples were resolved on 4-20% Mini-PROTEAN® TGX™ Precast Protein Gels (Bio-Rad, 4568096) or 12% polyacrylamide gels and transferred to nitrocellulose membranes. Immunoblotting is as below.

Immunoblotting. Whole cell lysates containing SDS buffer were homogenized with a 27-G syringe and resolved on 4-20% Mini-PROTEAN® TGX™ Precast Protein Gels (Bio-Rad, 4568096) or 6/10/12% home-made polyacrylamide gels and transferred to nitrocellulose membranes (Fisher Scientific, 45004002). Membranes were washed in Tris-buffered saline (TBS) containing 0.1% Tween® 20 (TBS-T) and blocked with TBS-based blocking buffer (LI-COR). Membranes were incubated with primary antibodies, washed again, incubated with species-specific secondary antibodies. For immunoprecipitation blots, Membranes were washed and blocked as above. Membranes were incubated with primary antibodies, washed again, incubated with species-specific, light chain-specific secondary antibodies (Jackson ImmunoResearch Labs, 115-655-174 and 211-622-171). Blots were analyzed using LI-COR imaging.

In vitro co-immunoprecipitation. HEK293T were grown in DMEM with 10% FBS. Cells were transfected with pCMV 3xFlag-SPAK 50-545 (human) or Myc-AS160 (residues 193-446). Cells were washed and resuspended in 5 ml cold phosphate-buffered saline (PBS) with 200 μM PMSF and 1:1000 protease inhibitor cocktail (PBSii) as above. 1 ml of 3xFlag-SPAK supernatant was mixed with 30 μl of anti-Flag magnetic agarose beads (Pierce A36797) and incubated at 4°C for 1hr, washed 3X with 1 ml cold PBSii using magnetic rack, followed by addition of 0.5 ml supernatant Myc-AS160 193-446. The sample was divided in half and 100 μM NH_3^+-SAGRRFIVSPVPE-COO^- blocking peptide diluted in 25 mM Tris-HCl pH 7.75, 125 mM NaCl was added to one of two and incubated at 4°C for 1hr. Samples were washed 3X with 1 ml cold PBSii. Myc-AS160 193-446 was eluted by addition of 45 μl of 500 μM blocking peptide and 15 μl 5X sample buffer was added to the eluant. Bait and prey proteins were loaded on separate gels (Bio-Rad 4-20% precast gels cat. #4568094). Proteins were transferred to nitrocellulose

membrane and immunoblotted as described above. The mouse monoclonal Myc antibody was from clone 9E10. Blots were washed 3 x 20 ml with TBS-T then incubated with 1:5000 IRDye 680 goat anti-Mouse secondary antibody (LI-COR # 926-68070) and analyzed by LI-COR imaging.

Fluorescence Polarization. 3.0 μM His_6-OSR1 CCT was mixed with 25 nM NH_3^+-NLVGRF[DAP-FAM]VSPVPE-COO^- (DAP-FAM: 2,3-diaminopropionic acid, unnatural amino acid, conjugated to FAM) in 25 mM Tris-HCl pH 7.75 (at 25° C), 125 mM NaCl, and 1 mM DTT. Unlabeled competing peptides were then added and subjected to a 2-fold stepwise dilution. Fluorescence polarization measurements were carried out on a BioTek Synergy H1 multi-mode plate reader equipped with a fluorescein polarizing filter cube (Em: 485 nm, Ex: 528 nm, 510 nm dichroic mirror). Data was fit to a model of one-site competitive binding to determine K_i using GraphPad Prism software.

Immunofluorescence. SH-SY5Y cells were fixed on glass coverslips (Fisher Scientific, 12-545-80) with 4% paraformaldehyde for 20min at room temperature, washed with PBS and blocked in 10% normal goat serum (Life Technologies, 50-062Z) before incubating with primary antibodies for 1hr at room temperature. After washing with PBS, cells were incubated with an Alexa Fluor® 488 conjugated goat-anti-mouse secondary antibody (Thermo Fisher Scientific, A11029) and Alexa Fluor® 594 conjugated goat-anti-rabbit secondary antibody (Thermo Fisher Scientific, A11037). Slides were mounted with DAPI Fluoromount-G (Thermo Fisher Scientific, 00-4959-52). Immunofluorescent images were acquired on a Zeiss LSM880 inverted confocal microscope (Carl Zeiss, Oberkochen, Germany). Images were deconvolved using AutoQuant® software (Media Cybernetics, USA). The colocalizing pixels were identified and Pearson's correlation coefficient was determined using Imaris software (Oxford Instruments).

***In vitro* glucose uptake assay.** Cells were placed in DMEM without serum and with DMSO or WNK463 for 2hr and then treated with insulin with or without WNK463 for 20min. A mixture of 0.625 μCi [^{3}H]-2-deoxyglucose and unlabeled 2-deoxyglucose (1 mM) was added for 30min at 37°C. After rinsing, cells were lysed, and radioactivity was measured using a scintillation counter. The amount of radioactivity is directly proportional to the rate of glucose utilization [20].

Surface biotinylation in SH-SY5Y cells. Biotinylation experiments were as described previously [179]. Differentiated SH-SY5Y cells in serum-free medium were pre-treated with WNK463 or DMSO for 2hr and treated with insulin with or without WNK463 for 30min. Cells were biotinylated at 4°C with NHS-SS-biotin (0.9 mg/ml) in 10 mM HEPES, 130 mM NaCl, 2 mM $MgSO_4$, 1 mM $CaCl_2$, 5.5 mM glucose for 15min. After rinsing in 25 mM glycine, cells were lysed

in 150 mM NaCl, 50 mM HEPES (pH 7.5), 5 mM EDTA, 1% Triton X-100, 0.2% SDS, and protease inhibitors as above. Lysates were incubated with streptavidin-agarose beads (Pierce Biotechnology) at 4°C overnight. Beads were washed, and biotinylated proteins were extracted by boiling in 60 µl SDS sample buffer with 100 mM dithiothreitol and 5% β-mercaptoethanol. Proteins extracted from the beads (surface) along with total protein were resolved by SDS-PAGE (6% gels). GLUT4 and GAPDH were detected by Western blotting.

Hippocampal slice culture. Organotypic hippocampal slice cultures were prepared from postnatal day 5 (P5) C57BL/6 mouse strain (Jackson Laboratories, Bar Harbor, ME) and incubated in Minimum Essential Medium (MEM: Gibco, 51200-038) with 5% HyClone Donor Equine Serum (Cytiva, SH30074.03) using previously published protocols [176]. Slices were incubated with WNK463 or DMSO for 1hr. A mixture of 0.625 µCi [^{3}H]-2-deoxyglucose and unlabeled 2-deoxyglucose (1 mM) was added for 1min at 37°C. Slices were placed on ice and washed 4X with ice-cold MEM medium. Slices were homogenized in mortar and pestle and radioactivity was measured using a liquid scintillation counter.

Animal studies. All animal studies were performed according to UTSW Institutional Animal Care and Use Committee guidelines. For harvesting hippocampus from P0-P1 WT C57BL/6J mice for primary cultures, mice were anesthetized by hypothermia followed by decapitation. For other terminal experiments, the method of euthanasia for harvesting tissues was ketamine/xylazine (IP) followed by decapitation for Western blots or [^{3}H]-2-deoxyglucose assay. For behavioral and *in vivo* glucose uptake assay, mice were weighed (~25 g) and orally gavaged daily with 200 µl WNK463 dissolved in 1% DMSO or formulated as a suspension in 0.5:0.5:99 (w:w:w) 2-hydroxypropyl β-cyclodextrin: Pluronic F68: purified water at 6 mg/kg, as indicated.

***In vivo* glucose uptake assay.** 1 µCi/g body weight of [^{3}H]-2-deoxyglucose was administered into mice by intraperitoneal (IP) injection. After 45min, mice were anesthetized with xylazine/ketamine and decapitated. Brains were removed and immediately placed on ice and hippocampi were dissected and homogenized. The radioactivity was measured using liquid scintillation counter. Plasma samples were taken immediately before mice are sacrificed and radioactivity was analyzed to ensure no significant differences in [^{3}H]-2-deoxyglucose [20]. The amount of radioactivity (nCi/g) is directly proportional to the rate of glucose utilization.

Crude Synaptosome preparation. Crude synaptosomes were prepared as in [180]. C57BL/6J mice were anesthetized as above, brains were removed, and cerebrum dissected and homogenized with mortar and pestle in 0.32 M sucrose, 10 mM HEPES pH 7.4. The

homogenates were centrifuged at 1000 x g for 10min at 4 °C and the pellet was removed. The supernatant was centrifuged at 17,000 x g for 30min at 4 °C. This second pellet contained the crude synaptosome fraction and was resuspended in Krebs-Ringer Bicarbonate HEPES buffer (KRBH) buffer containing: 5 mM KCl, 120 mM NaCl, 15 mM HEPES pH-7.4, 24 mM $NaHCO_3$, 1 mM $MgCl_2$, 2 mM $CaCl_2$ (no glucose) and incubated with WNK463 or DMSO for 1hr. A mixture of 0.625 µCi [^{3}H]-2-deoxyglucose and unlabeled 2-deoxyglucose (1 mM) was added for 1min at 37°C. Cells were placed on ice and washed 4X with ice-cold KRBH. After sedimentation at 21,000 x g for 15min, radioactivity in the pellet fraction was measured using a liquid scintillation counter.

Surface biotinylation in brain slices. Biotinylation experiments were performed as described previously [177]. From two mice, 4-5 slices were pooled together randomly for each condition. After a 2-3 h recovery period in aCSF, slices were treated with aCSF containing either DMSO or WNK463 (1 µM) for 45min at 30°C. Slices were treated for 45min with aCSF containing DMSO or WNK463 with or without insulin (10 nM). At the end of the treatment, slices were placed on ice to stop endocytosis and were washed with ice-cold aCSF containing 0.9 mg/ml sulfo-NHS-SS-biotin (Thermo Fisher scientific) for 15min. To quench the biotin reaction, slices were washed once with ice-cold aCSF followed by aCSF containing glycine (25 mM) for 15min and then again with aCSF alone. The hippocampus was dissected from each cerebral slice and homogenized in a modified radioimmunoprecipitation assay (RIPA) buffer containing: 50 mM Tris-HCl, pH 7.4, 1% Triton X-100, 0.1% SDS, 0.5% Na-deoxycholate, 150 mM NaCl, 2 mM EDTA, 50 mM NaH_2PO_4, 50 mM NaF, 10 mM $Na_4P_2O_7$, 1 mM Na_3VO_4, and protease inhibitor cocktail as above, followed by sonication. Homogenates were centrifuged at 14,000x g for 10min at 4°C. Protein concentration was measured using BCA Protein Assay (Fisher Scientific, PI23227). 20 µg of protein was removed for total protein measurements. 200 µg protein was then mixed with 200 µl of streptavidin-agarose beads (Thermo Fisher Scientific) by rotating for 2 h at 4°C. The beads were washed twice with 4X volumes of RIPA buffer. Both total and biotinylated (surface) proteins were resolved by 4-20% SDS-PAGE, transferred to nitrocellulose membranes. GAPDH and GLUT4 were detected by Western Blot.

Open Field test. Mice were placed in the periphery of a novel open field environment (44 cm x 44 cm, walls 30 cm high) in a dimly lit room (approximately 67 lux) and allowed to explore for 10min. The animals were monitored from above by a video camera connected to a computer running video tracking software (Ethovision XT V-17, Noldus, Leesburg, Virginia) to determine the time, distance moved and number of entries into two areas: the periphery (5 cm from the

walls) and the center (14 cm x 14cm). The drug or vehicle was given every day for 3 days prior to testing and was last given 15hr prior to the test. In mice pre-exposed to electric shocks, they received three 0.5 mA foot-shocks at 1min intervals in the fear-conditioning chamber one day before the Open Field test.

Elevated Plus Maze test. Mice were placed in the center of a black plastic elevated plus maze (each arm 30 cm long and 5 cm wide with two opposite arms closed by 25 cm high walls) elevated 31 cm in a dimly lit room (approximately ~67 Lux) and allowed to explore for 5min. The animals were monitored from above by a video camera connected to a computer running video tracking software (Ethovision XT V-17, Noldus, Leesburg, Virginia) to determine time spent in the open and closed arms, time spent in the middle, and the number of entries into the open and closed arm. The drug or vehicle was given every day for 3 days prior to testing and was last given 15hr prior to the test. In mice pre-exposed to electric shocks, they received three 0.5 mA foot-shock, 1min interval in the fear-conditioning chamber one day before the Elevated Plus Maze test.

Fear Conditioning test. Fear conditioning was measured in boxes equipped with a metal grid floor connected to a scrambled shock generator (Med Associates Inc., St. Albans). For training, mice were individually placed in the chamber. After 2min, the mice received 3 tone-shock pairings (30s white noise, 80 dB tone co-terminated with a 2s, 0.5 mA foot-shock, 1min intertrial interval). The following day, memory of the context was measured by placing the mice into the same chambers and freezing was measured automatically by the Med Associates software for 5min. 48hr after training, memory for the white noise cue was measured by placing the mice in a box with altered floors and walls, different lighting, and a vanilla smell. Freezing was measured for 3min, then the noise cue was turned on for an additional 3min and freezing was measured. Mice received oral WNK463 or vehicle 3 days prior to the start of the test and continued until the completion of the test.

Novel Object test. The mice were individually habituated to the test arena (similar to that as the open field test arena) for 2 consecutive days with two identical objects. On the third day, the mice were allowed to explore a different set of similar objects for up to 15min (training). Training concluded when the mouse explored the objects for a total of 30s (both objects combined). Mice that failed to explore the objects for at least 30s were excluded from the study. 6hr after training, a test was performed where one of the familiar objects from testing was replaced by a novel object. Mice received 2 days of daily oral WNK463 or vehicle by oral gavage prior to the start of the test and continued until the completion of the test. Time spent exploring the familiar (a) and

the novel object (b) was measured. The discrimination index was calculated by the formula (b – a)/(b + a). Mice were excluded from analysis when the total exploration time (b + a) during testing was less than 30s.

Locomotor Activity test. Mice were placed individually into a clean, plastic mouse cage (18 cm x 28 cm) with minimal bedding. Each cage was placed into a dark Plexiglas box. Movement was monitored by photobeams (Photobeam Activity System, San Diego Instruments, San Diego, CA) for 5hr, with the number of beam breaks recorded every 30min. Mice received 2 days of daily oral WNK463 or vehicle prior to the start of the test.

Materials, Drugs and Reagents. WNK463 (Selleck Chemicals, S8358), anti-Vinculin antibody (Sigma Aldrich, V9131), anti-pOSR1/pSPAK antibody (EMD Millipore, 07-2273), anti-OSR1 polyclonal antibody (Cell Signaling, 3729S), anti-OSR1 monoclonal antibody (VWR, 10624-616), anti-WNK1 antibody (Cell Signaling, 4979S), anti-pAKT S473 antibody (Cell Signaling Technology, 4060S), anti-pAKT T308 antibody (Cell Signaling Technology, 4056S), anti-AKT1 antibody (Cell Signaling Technology, 2920S), anti- GAPDH antibody (Cell signaling Technology, 97166L), anti-GLUT4 polyclonal antibody (ab33780, Abcam), anti-GLUT4 monoclonal antibody (MA5-17176), anti-AS160 antibody (Cell Signaling Technology, 2670S), anti-pAS160 S588 antibody (50-191-485, Fisher Scientific), anti-sortilin antibody (MABN1792, Sigma-Aldrich), anti-Flag antibody (Sigma-Aldrich, F1804). The Myc antibody was a monoclonal from mouse 9E10 (antibody no longer commercially available). Q256 WNK1 antibody was homemade as in [73], Optimem (Invitrogen, 51985-034), Lipofectamine 2000 (Life Technologies, 11668019).

Statistics and Reproducibility. The data are presented as mean±SEM from at least two-three independent experiments. Micrographs are representative images from at least three experiments. For the quantification of immunofluorescence images, the number of cells used for each representative experiment is indicated and p values between two groups were determined using unpaired t-tests. Single intergroup comparisons between 2 groups were performed with 2-tailed Student's *t*-test as specifically mentioned in each case. $p < 0.05$ was considered statistically significant.

Inclusion and Exclusion criteria. Mice showing at least 50% decrease in phospho-OSR1 levels in the hippocampal lysates were included and used for analysis. No outliers were excluded from the study. Randomization: For inhibitor treatment, mice were randomized before grouping. Blinding: In cases where manual scoring of the behavior was involved, the analysis was performed by an associate blinded to the identity of the mice. Power analysis: On the basis

of previous experience of the rodent behavioral core with C57BL/6J mice, animal cohorts of 6-11 mice per group are sufficient to detect differences between groups with a 90% power and a 5% type I error rate.

Data Sharing. We will follow all NIH policies with respect to sharing reagents, materials, and information with other investigators. Detailed protocols are provided to everyone who requests them. Upon publication, this manuscript will be submitted to the National Library of Medicine's PubMed Central as outlined by NIH policy.

Acknowledgements

The authors thank the members of Cobb and Huber labs for valuable suggestions, and Dionne Ware for administrative assistance. We would like to thank Dr. Joseph Albanesi, Department of Pharmacology, University of Texas Southwestern Medical Center, for discussions and suggestions related to the manuscript and figures. We would like to thank Steve Stippec (Cobb lab) for his help with molecular cloning of constructs used in this study. We would like to thank Gemma Molinaro and Julia Wilkerson (Huber lab) for providing technical support with primary neuronal/glial cell culture, hippocampal slice culture and preparation of hippocampal slices for surface biotinylation experiments. We would also like to thank Barbara Barylko, Department of Pharmacology, University of Texas Southwestern Medical Center for assistance with crude synaptosome preparation and Jenna Jewell, Department of Molecular Biology, University of Texas Southwestern Medical Center, for HEK293 cells. These studies were supported by NIH K99AG075161-01A1 to ABJ, NIH R01 HL147661 to MHC, Welch Foundation grant I1243 to MHC, and 1R37NS114516-01A1 to KH. Behavioral experiments were performed in collaboration with Rodent Behavior Core, (supported in part by the Peter O'Donnell Jr. Brain Institute, University of Texas Southwestern Medical Center). The authors would also like to acknowledge the assistance of the UT Southwestern Live Cell Imaging Facility, a shared resource of the Harold C. Simmons Comprehensive Cancer Center, supported in part by an NCI Cancer Center Support Grant, 1P30 CA142543-01 and NIH Shared Instrumentation Award 1S10 OD021684-01 to Dr. Kate Luby-Phelps (LSM880 Airyscan).

Author Contributions. ABJ: Conceptualized, supervised, designed and performed experiments, performed analysis, wrote manuscript, generated initial figures; **AA**: performed experiments; **DB**: performed experiments; **CAT**: performed experiments; **SGB**: Experiment

design; **KH**: Supervision and acquired funding; **MHC**: Supervision, acquired funding, edited manuscript.

Declaration of interests. The authors declare no competing interests.

Figure Legends

Figure 1. Inhibition of WNK in mice enhances learning and memory. A) Model shows WNK downstream signaling. **B)** Quantification shows pOSR1 (Ser325)/total OSR1 from hippocampi of mice treated with WNK463 (PO; 6 mg/kg) or vehicle; n=4. **C)** Diagram representing Novel Object Recognition test protocol. **D)** Quantification of discrimination index in mice administered with WNK463 (PO; 6mg/kg) (n=13) or vehicle (n=19) tested on the Novel Object Recognition protocol. **E)** Diagram representing Context-Cue Fear Conditioning test protocol. **F)** Quantification of % Freezing in Contextual Fear Conditioning test in mice administered WNK463 (PO; 6 mg/kg) (n=11) or vehicle: n=9. **G)** Quantification of % Freezing in Cued Fear Conditioning test in mice administered WNK463 (PO; 6mg/kg) (n=11) or vehicle: n=9. **H)** Diagram representing locomotor test protocol. **I)** Quantification of locomotory activity in mice administered WNK463 (PO; 6mg/kg) or vehicle; n=6. **J)** Model shows the effect of WNK inhibition on learning and memory in mice. Data are represented as Mean±SE; analyzed by unpaired two-tailed Student's *t*-test or one-way ANOVA. ns: non-significant, *p<0.05, **p<0.005 and *** p<0.0005. Graphics created with BioRender.com.

Figure 2. Inhibition of hippocampal WNK enhances anxiety-related behavior in mice. A) Diagram representing Open Field test protocol. **B)** Graph representing cumulative time spent in the center by mice treated with vehicle or WNK463 (PO; 6 mg/kg) in the Open Field test; n=7. **C)** Graph representing the number of entries (frequency) in the center by mice treated with vehicle or WNK463 (PO; 6 mg/kg) in the Open Field test; n=7. **D)** Diagram representing Elevated Plus Maze test protocol. **E)** Graph representing cumulative time spent in the open arms by mice treated with vehicle or WNK463 (PO; 6 mg/kg) in the Elevated Plus Maze test; n=8. **F)** Graph representing the number of entries (frequency) in the open arms by mice treated with vehicle or WNK463 (PO; 6 mg/kg) in the Elevated Plus Maze; n=8. **G)** Graph representing cumulative time spent in the center by mice treated with vehicle (n=8) or WNK463 (PO; 6 mg/kg) (n=7) in the Open Field test after mice received electric foot-shocks. **H)** Graph representing the number of entries (frequency) in the center by mice treated with vehicle (n=8) or WNK463 (PO; 6 mg/kg) (n=7) in the Open Field test after mice received the electric foot-shocks. **I)** Graph representing cumulative time spent in the open arms by mice treated with vehicle (n=7) or WNK463 (PO; 6 mg/kg) (n=6) in the Elevated Plus Maze test after mice

received electric foot-shocks. **J)** Graph representing the number of entries (frequency) in the open arms by mice treated with vehicle (n=7) or WNK463 (PO; 6 mg/kg) (n=6) in the Elevated Plus Maze after mice received electric foot-shocks. Data are represented as Mean±SE; analyzed by unpaired two-tailed Student's *t*-test or one-way ANOVA. *p<0.05, **p<0.005 and *** p<0.0005. ns: non-significant; p>0.05.

Figure 3. Inhibition of WNK augments glucose uptake via GLUT4. A) Model shows downstream effects of insulin and the impact of WNKs on insulin signaling. **B)** Graph representing quantification of *in vivo* radioactive 2-deoxyglucose uptake per mg hippocampal weight in mice treated with vehicle or WNK463 (PO; 6 mg/kg); n=4. **C)** Graph representing enhanced radioactive 2-deoxyglucose uptake in hippocampal slice culture from C57BL/6J whole brains treated with WNK63 (1 μM); n=4. **D)** Graph representing enhanced radioactive 2-deoxyglucose uptake in crude synaptosome from C57BL/6J whole brains treated with WNK63 (1 μM); n=3. **E)** Graph shows *in vitro* radioactive 2-deoxyglucose uptake in SH-SY5Y cells treated with WNK463 (1 μM), insulin (10 nM); n=7. **F)** Graph representing enhanced radioactive *in vitro* 2-deoxyglucose uptake in differentiated SH-SY5Y cells treated with insulin (10 nM) ± WNK463 (1 μM) ± indinavir (10 nM); n=5. **G)** Representative Western blot shows surface and total GLUT4 protein fraction from mice hippocampal slices treated with insulin (10 nM) and/or WNK463 (1 μM). **H)** Corresponding quantification of 'G' shows enhanced surface GLUT4 (measured as a fraction of total GLUT4) with WNK463 ± insulin treatment; n=4. Data are represented as Mean±SE; analyzed by unpaired two-tailed Student's *t*-test or one-way ANOVA. *p<0.05, **p<0.005 and *** p<0.0005. Graphics created with BioRender.com.

Figure 4. Inhibition of WNK enhances insulin signaling in the hippocampus and cell culture. A) Model shows insulin signaling and the impact of WNK kinases on insulin signaling. **B)** Quantification of pAKT/AKT from hippocampi of mice treated with WNK463 (PO; 6 mg/kg) or vehicle; n=4. **C)** Representative Western blot shows pAKT, AKT and pOSR1 in the presence of WNK463 (1 μM) ± insulin (10 nM) in SH-SY5Y cells. **D)** Quantification of pAKT/AKT in differentiated SH-SY5Y cells treated with insulin (10 nM) ± WNK463 (1 μM); n=4. **E)** Representative Western blot shows pAKT and GAPDH in presence of WNK463 (1 μM) ± insulin (10 nM) in mouse cortical primary cells. **F)** Quantification of pAKT/GAPDH in cortical primary cells treated with insulin (10 nM) ± WNK463 (1 μM); n=2 for DMSO and insulin and n=3 for WNK463±insulin. Data are represented as Mean±SE; analyzed by unpaired two-tailed Student's *t*-test or one-way ANOVA. *p<0.05, **p<0.005 and *** p<0.0005. Graphics created with BioRender.com.

Figure 5. OSR1 interacts with molecular mediators involved in GLUT4 trafficking. A) Model shows balanced regulation of sortilin and AS160 by the WNK/OSR1/SPAK pathway to regulate GLUT4 trafficking. **B)** Representative Western Blot shows co-immunoprecipitation of endogenous OSR1 with AS160 from whole brain C57BL/6J mouse lysates; n=3. **C)** Representative Western blot shows co-immunoprecipitation of AS160 with OSR1 upon treatment with WNK63 (1 μM) and/or insulin (10 nM) in differentiated SH-SY5Y cells. **D)** Corresponding quantification of '**C**' shows decreased association of AS160 and OSR1 in cells treated with insulin (10 nM) + WNK463 (1 μM) compared to insulin alone; n=6. **E)** Representative Western blot shows pAS160, AS160 and GAPDH in differentiated SH-SY5Y cells treated with insulin (10 nM) ± WNK463 (1 μM). **F)** Corresponding quantification of 'E' shows increased pAS160 in cells treated with insulin (10 nM) or WNK463 (1 μM) compared to DMSO; n=4. **G)** R-x-F-x-V- containing blocking peptide (BP: WNK1 1253-1265; NH_3^+-SAGRRFIVSPVPE-COO^-; 100 μM) decreases interaction of overexpressed OSR1/SPAK CCT bait protein fragment (aa 50-545) with myc-AS160 protein fragment (aa 193-446) *in vitro*; n=3. **H)** Corresponding quantification of 'G'. **I)** Bright-field (left) or confocal images shows co-localization of endogenous OSR1 with sortilin in differentiated SH-SY5Y cells. OSR1 (red), sortilin (green), merged (yellow), scale bar=10 μm; n=3. **J)** Representative endogenous co-immunoprecipitation of OSR1 with sortilin in differentiated SH-SY5Y cells; n=5. **K)** Yeast two-hybrid assay shows binding of the conserved C-terminus (CCT) of OSR1 with the C-terminus (C-t) of sortilin (3); binding of full-length and CCT of OSR1 to the C-terminus of WNK1 as positive controls (5,7). N-t: N-terminus. **L)** Representative Western blot shows co-immunoprecipitation of OSR1 and Flag-sortilin in HEK cells is diminished upon co-incubation with the blocking peptide (BP) SAGRRFIVSPVPE; n=3. **M)** Corresponding graphical representation for 'L'; n=8. Data are represented as Mean±SE; analyzed by unpaired two-tailed Student's *t*-test or one-way ANOVA. *p<0.05, **p<0.005 and *** p<0.0005. Graphics created with BioRender.com.

Supplementary Figure Legends

Supplementary Figure 1. **A)** Representative Western blot shows change in body weights of C57BL/6J mice treated with vehicle or WNK463 (PO; 6mg/kg) for 1 week; n=10. Data are represented as Mean±SE; analyzed by unpaired two-tailed Student's *t*-test. ns: non-significant; p>0.05.

Supplementary Figure 2. A) Quantification of total exploration time during Novel Object Recognition test protocol in mice administered with WNK463 (PO; 6 mg/kg); n=13 or vehicle;

n=19. Data are represented as Mean±SE; analyzed by unpaired two-tailed Student's *t*-test. ns: non-significant; p>0.05.

Supplementary Figure 3. A) Quantification of total distance moved (cm) in the Open Field test in mice administered with WNK463 (PO; 6 mg/kg) or vehicle; n=7. **B)** Quantification of total distance moved (cm) in the Open Field test in mice administered with WNK463 (PO; 6 mg/kg) (n=7) or vehicle (n=8) in mice pre-exposed to electric foot-shocks. **C)** Quantification of total distance moved (cm) in the Elevated Plus Maze test in mice administered with WNK463 (PO; 6 mg/kg) or vehicle; n=8. **D)** Quantification of total distance moved (cm) in the Elevated Plus Maze test in mice administered with WNK463 (PO; 6 mg/kg) or vehicle in mice pre-exposed to electric foot-shocks; n=7. Data are represented as Mean±SE; analyzed by unpaired two-tailed Student's *t*-test. *p<0.05, **p<0.005 and *** p<0.0005. ns: non-significant; p>0.05.

Supplementary Figure 4. A) Representative Western blot shows surface and total GLUT4 protein fraction in differentiated SH-SY5Y cells treated with insulin (10 nM) and/or WNK463 (1 μM). **B)** Corresponding quantification of 'A' shows enhanced surface GLUT4 (measured as a fraction of total GLUT4) with WNK463 ± insulin treatment; n=3. Data are represented as Mean±SE; analyzed by unpaired two-tailed Student's *t*-test. *p<0.05, **p<0.005 and *** p<0.0005.

Supplementary Figure 5. A) Graph representing the binding affinities of WT- sortilin and sortilin mutant peptides with OSR1/SPAK CCT determined by fluorescence anisotropy. Unlabeled peptides displace labeled peptide ($NH3^{+}$-NLVGRF-[DAP-FAM]-VSPVPE-COO^{-}) [diaminopropionic acid (DAP)]. Labeled peptide held constant at 25 nM, OSR1 CCT held constant at 3.0 μM; n=3.

References

1) Seaquist ER, Damberg GS, Tkac I, Gruetter R. The Effect of Insulin on In Vivo Cerebral Glucose Concentrations and Rates of Glucose Transport/ Metabolism in Humans. Diabetes. 2001;50(10)2203-2209.
2) Hasselbalch SG, Knudsen GM, Videbaek C, Pinborg LH, Schmidt JF, Holm S, Paulson OB. No effect of insulin on glucose blood-brain barrier transport and cerebral metabolism in humans. Diabetes. 1999;48(10):1915-21.
3) Leloup C, Arluison M, Kassis N, Lepetit N, Cartier N, Ferré P, Pénicaud L. Discrete brain areas express the insulin-responsive glucose transporter GLUT4. Brain Res Mol Brain Res. 1996;38(1):45-53.
4) Ren H, Yan S, Zhang B, Lu TY, Arancio O, Accili D. Glut4 expression defines an insulin-sensitive hypothalamic neuronal population. Mol Metab. 2014;3(4):452-459.
5) Mari Kobayashi, Hideki Nikami, Masami Morimatsu, Masayuki Saito. Expression and localization of insulin-regulatable glucose transporter (GLUT4) in rat brain. Neuroscience Letters. 1996;213(2):103-106.
6) Dore S, Kar S, Rowe W, Quirion R. Distribution and levels of 125I-IGF1, 125I-IGF2 and 125I-insulin receptor binding sites in the hippocampus of aged memory-unimpaired and -impaired rats. Neuroscience. 1997;80: 1033-1040.
7) Vannucci SJ, Koehler-Stec EM, Li K, Reynolds TH, Clark R, Simpson IA. GLUT4 glucose transporter expression in rodent brain: effect of diabetes. Brain Res. 1998;797(1):1-11.
8) McEwen BS, Reagan L. Glucose transporter expression in the central nervous system: Relationship to synaptic function. European Journal of Pharmacology. 2004;490(1-3):13-24.
9) Govers R, Coster AC, James DE. Insulin increases cell surface GLUT4 levels by dose dependently discharging GLUT4 into a cell surface recycling pathway. Mol Cell Biol. 2004 Jul;24(14):6456-66.
10) Muretta JM, Romenskaia I, Mastick CC. Insulin releases Glut4 from static storage compartments into cycling endosomes and increases the rate constant for Glut4 exocytosis. J Biol Chem. 2008 Jan 4;283(1):311-23.
11) Bakirtzi K, Belfort G, Lopez-Coviella I, Kuruppu D, Cao L, Abel ED, Brownell AL, Kandror KV. Cerebellar neurons possess a vesicular compartment structurally and functionally similar to Glut4-storage vesicles from peripheral insulin-sensitive tissues. J Neurosci. 2009 Apr 22; 29(16): 5193-201.
12) Piroli GG, Grillo CA, Reznikov LR, Adams S, McEwen BS, Charron MJ, Reagan LP. Corticosterone impairs insulin-stimulated translocation of GLUT4 in the rat hippocampus. Neuroendocrinology. 2007;85(2):71-80.
13) Grillo CA, Piroli GG, Hendry RM, Reagan LP. Insulin-stimulated translocation of GLUT4 to the plasma membrane in rat hippocampus is PI3-kinase dependent. Brain Res. 2009;1296:35-45.
14) Benomar Y, Naour N, Aubourg A, Bailleux V, Gertler A, Djiane J, Guerre-Millo M, Taouis M. Insulin and Leptin Induce Glut4 Plasma Membrane Translocation and Glucose Uptake in a Human Neuronal Cell Line by a Phosphatidylinositol 3-Kinase-Dependent Mechanism. Endocrinology. 2006;147(5):2550–2556.
15) Ashrafi G, Wu Z, Farrell RJ, Ryan TA. GLUT4 mobilization supports energetic demands of active synapses. Neuron. 2017;93: 606-615. e603

16) Fernando RN, Albiston AL, Chai SY. The insulin-regulated aminopeptidase IRAP is colocalised with GLUT4 in the mouse hippocampus--potential role in modulation of glucose uptake in neurones? Eur J Neurosci. 2008;28(3):588-98.
17) Ismail MA, Mateos L, Maioli S, Merino-Serrais P, Ali Z, Lodeiro M, Westman E, Leitersdorf E, Gulyás B, Olof-Wahlund L, Winblad B, Savitcheva I, Björkhem I, Cedazo-Mínguez A. 27-Hydroxycholesterol impairs neuronal glucose uptake through an IRAP/GLUT4 system dysregulation. J Exp Med. 2017;214(3):699-717.
18) Pearson-Leary J, McNay EC. Novel Roles for the Insulin-Regulated Glucose Transporter-4 in Hippocampally Dependent Memory. Journal of Neuroscience. 2016;36(47):11851-11864.
19) McNay EC, Pearson-Leary J. GluT4: A central player in hippocampal memory and brain insulin resistance. Experimental Neurology. 2020;323: 113076.
20) Pearson-Leary J, Jahagirdar V, Sage J, McNay EC. Insulin modulates hippocampally-mediated spatial working memory via glucose transporter-4. Behav Brain Res. 2018;338: 32-39.
21) McNay EC, Ong CT, McCrimmon RJ, Cresswell J, Bogan JS, Sherwin RS. Hippocampal memory processes are modulated by insulin and high-fat-induced insulin resistance. Neurobiology of Learning and Memory. 2010;93(4):546-553.
22) Park CR, Seeley RJ, Craft S, Woods SC. Intracerebroventricular insulin enhances memory in a passive avoidance task. Physiology and Behaviour, 68 (2000), 509-514
23) Zhao W, Chen H, Xu H, Moore E, Meiri N, Quon MJ, Alkon DL. Brain insulin receptors and spatial memory. Correlated changes in gene expression, tyrosine phosphorylation, and signaling molecules in the hippocampus of water maze trained rats. J Biol Chem. 1999;274(49):34893-902.
24) Babri S, Badie HG, Khamenei S, Seyedlar MO. Intrahippocampal insulin improves memory in a passive-avoidance task in male wistar rats. Brain Cogn. 2007 Jun;64(1):86-91.
25) Zhao WQ, Chen H, Quon MJ, Alkon DL. Insulin and the insulin receptor in experimental models of learning and memory. Eur J Pharmacol. 2004 Apr 19;490(1-3):71-81.
26) Kern W, Peters A, Fruehwald-Schultes B, Deininger E, Born J, Fehm HL. Improving influence of insulin on cognitive functions in humans. Neuroendocrinology. 2001 Oct;74(4):270-80.
27) Soto M, Cai W, Konishi M, Kahn CR. Insulin signaling in the hippocampus and amygdala regulates metabolism and neurobehavior. PNAS. 2019;116(13):6379-6384.
28) Kleinridders A, Pothos EN. Impact of Brain Insulin Signaling on Dopamine Function, Food Intake, Reward, and Emotional Behavior. Curr Nutr Rep. 2019;8(2):83-91.
29) Craft S, Newcomer J, Kanne S, Dagogo-Jack S, Cryer P, Sheline Y, Luby J, Dagogo-Jack A, Alderson A. Memory improvement following induced hyperinsulinemia in Alzheimer's disease. Neurobiol Aging. 1996;17(1):123-30.
30) McNay EC, Fries TM, Gold PE. Decreases in rat extracellular hippocampal glucose concentration associated with cognitive demand during a spatial task. PNAS. 2000;97: 2881-2885.
31) Long JM, Davis BJ, Garofalo P, Spangler EL, Ingram DK. Complex maze performance in young and aged rats: response to glucose treatment and relationship to blood insulin and glucose. Physiol Behav. 1992 Feb;51(2):411-8.

32) McNay EC, Gold PE. Food for thought: Fluctuations in brain extracellular glucose provide insight into the mechanisms of memory modulation. Cognitive and Behavioural Neuroscience Reviews. 2002;1(4): 264-280.
33) Suwa M, Yamamoto KI, Nakano H, Sasaki H, Radak Z, Kumagai S. Brain-derived neurotrophic factor treatment increases the skeletal muscle glucose transporter 4 protein expression in mice. Physiol Res. 2010;59(4):619-623.
34) Mora S, Kaliman P, Chillarón J, Testar X, Palacín M, Zorzano A. Insulin and insulin-like growth factor I (IGF-I) stimulate GLUT4 glucose transporter translocation in Xenopus oocytes. Biochem J. 1995 Oct 1;311 (Pt 1)(Pt 1):59-65.
35) Dehvari N, Hutchinson DS, Nevzorova J, et al. beta(2)-Adrenoceptors increase translocation of GLUT4 via GPCR kinase sites in the receptor C-terminal tail. Br J Pharmacol 2012;165:1442–1456.
36) Li Y, Wang P, Xu J, Desir GV Voltage-gated potassium channel Kvl.3 regulates GLUT4 trafficking to the plasma membrane via a Ca2+-dependent mechanism. Am J Physiol Cell Physiol 2006;290:C345–351.
37) Tohda C, Nakanishi R, Kadowaki M. Hyperactivity, memory deficit and anxiety-related behaviors in mice lacking the p85alpha subunit of phosphoinositide-3 kinase. Brain Dev. 2009; 31: 69–74.
38) Giménez-Llort L, Santana-Santana M, Bayascas JR. The Impact of the PI3K/Akt Signaling Pathway in Anxiety and Working Memory in Young and Middle-Aged PDK1 K465E Knock-In Mice. Front Behav Neurosci. 2020 May 8;14:61.
39) Sandouk T, Reda D, Hofmann C. The antidiabetic agent pioglitazone increases expression of glucose transporters in 3T3-F442A cells by increasing messenger ribonucleic acid transcript stability. Endocrinology. 1993;133(1):352–359.
40) Farr SA, Poon HF, Dogrukol-Ak D, Drake J, Banks WA, Eyerman E, Butterfield DA, Morley JE. The antioxidants alpha-lipoic acid and N-acetylcysteine reverse memory impairment and brain oxidative stress in aged SAMP8 mice. J. Neurochem. 2003;84(5):1173–1183.
41) Christensen DP, Dahllof M, Lundh M, Rasmussen DN, Nielsen MD, Billestrup N, Grunnet LG, Mandrup-Poulsen T. Histone deacetylase (HDAC) inhibition as a novel treatment for diabetes mellitus. Mol. Med. 2011;17(5–6):378–390.
42) Kobilo T, Yuan C, van Praag H. Endurance factors improve hippocampal neurogenesis and spatial memory in mice. Learn. Mem. 2011;18(2):103–107.
43) Craft S, Watson GS. Insulin and neurodegenerative disease: shared and specific mechanisms. Lancet Neurol. 2004 Mar;3(3):169-78.
44) Kleinridders A, Cai W, Cappellucci L, Ghazarian A, Collins WR, Vienberg SG, Pothos EN, Kahn CR. Insulin resistance in brain alters dopamine turnover and causes behavioral disorders. Proc Natl Acad Sci U S A. 2015;112(11):3463-8.
45) Schubert M, Gautam D, Surjo D, Ueki K, Baudler S, Schubert D, Kondo T, Alber J, Galldiks N, Küstermann E, Arndt S, Jacobs AH, Krone W, Kahn CR, Brüning JC. Role for neuronal insulin resistance in neurodegenerative diseases. Proc Natl Acad Sci U S A. 2004;101(9):3100-5.
46) Campbell S, Macqueen G. The role of the hippocampus in the pathophysiology of major depression. J Psychiatry Neurosci. 2004;29(6):417-426.
47) Beauquis J, Roig P, Homo-Delarche F, De Nicola A, Saravia F. Reduced hippocampal neurogenesis and number of hilar neurons in streptozotocin-induced diabetic mice:

reversion by antidepressant treatment. European Journal of Neuroscience. 2006;23(6):1539–1546.
48) Gispen WH, Biessels GJ. Cognition and synaptic plasticity in diabetes mellitus. Trends Neurosci. 2000 Nov;23(11):542-9.
49) Kleinridders A, Cai W, Cappellucci L, Ghazarian A, Collins WR, Vienberg SG, Pothos EN, Kahn CR. Insulin resistance in brain alters dopamine turnover and causes behavioral disorders. Proc Natl Acad Sci U S A. 2015;112(11):3463-8.
50) Wijtenburg SA, Kapogiannis D, Korenic SA, Mullins RJ, Tran J, Gaston FE, Chen S, Mustapic M, Hong LE, Rowland LM. Brain insulin resistance and altered brain glucose are related to memory impairments in schizophrenia. Schizophrenia Research. 2019;208: 324-330.
51) Haley AP, Knight-Scott J, Simnad VI, Manning CA. Increased glucose concentration in the hippocampus in early Alzheimer's disease following oral glucose ingestion. Magn Reson Imaging. 2006 Jul;24(6):715-20.
52) Willette AA, Bendlin BB, Starks EJ, Birdsill AC, Johnson SC, Christian BT, Okonkwo OC, La Rue A, Hermann BP, Koscik RL, Jonaitis EM, Sager MA, Asthana S. Association of Insulin Resistance with Cerebral Glucose Uptake in Late Middle-Aged Adults at Risk for Alzheimer Disease. JAMA Neurol. 2015;72(9):1013-20.
53) Gold PE. Glucose and age-related changes in memory. Neurobiol Aging. 2005;26 Suppl 1:60-64.
54) Watson GS, Craft S. Modulation of memory by insulin and glucose: neuropsychological observations in Alzheimer's disease. Eur J Pharmacol. 2004;490(1-3):97-113.
55) Patel SS, Mehta V, Changotra H, Udayabanu M. Depression mediates impaired glucose tolerance and cognitive dysfunction: A neuromodulatory role of rosiglitazone. Horm Behav. 2016;78: 200-10.
56) Reagan LP. Glucose, stress and hippocampal neuronal vulnerability. Int. Rev. Neurobiol. 2002;51: 289-324
57) Kennedy SH, Evans KR, Krüger S, Mayberg HS, Meyer JH, McCann S, Arifuzzman AI, Houle S, Vaccarino FJ. Changes in regional brain glucose metabolism measured with positron emission tomography after paroxetine treatment of major depression. Am J Psychiatry. 2001;158(6):899-905.
58) Głombik K, Detka J, Góralska J, Kurek A, Solnica B, Budziszewska B. Brain Metabolic Alterations in Rats Showing Depression-Like and Obesity Phenotypes. Neurotox Res. 2020;37: 406–424.
59) Nishi H, Sawamoto N, Namiki C, Yoshida H, Dinh HD, Ishizu K, Hashikawa K, Fukuyama H. Correlation between cognitive deficits and glucose hypometabolism in mild cognitive impairment. J Neuroimaging. 2010 Jan;20(1):29-36.
60) Mosconi L, De Santi S, Li J, Tsui WH, Li Y, Boppana M, Laska E, Rusinek H, de Leon MJ. Hippocampal hypometabolism predicts cognitive decline from normal aging. Neurobiol Aging. 2008;29(5):676-92.
61) Zheng H, Zheng Y, Zhao L, Chen M, Bai G, Hu Y, Hu W, Yan Z, Gao H. Cognitive decline in type 2 diabetic db/db mice may be associated with brain region-specific metabolic disorders. Biochim Biophys Acta Mol Basis Dis. 2017 Jan;1863(1):266-273.
62) Steen E, Terry BM, Rivera EJ, Cannon JL, Neely TR, Tavares R, Xu XJ, Wands JR, de la Monte SM. Impaired insulin and insulin-like growth factor expression and signaling mechanisms in Alzheimer's disease--is this type 3 diabetes? J Alzheimers Dis. 2005;7(1):63-80.

63) Zisman A, Peroni OD, Abel ED, Michael MD, Mauvais-Jarvis F, Lowell BB, Wojtaszewski JF, Hirshman MF, Virkamaki A, Goodyear LJ, Kahn CR, Kahn BB. Targeted disruption of the glucose transporter 4 selectively in muscle causes insulin resistance and glucose intolerance. Nat Med. 2000 Aug;6(8):924-8.
64) Heaton RK, Clifford DB, Franklin DR Jr, Woods SP, Ake C, Vaida F, Ellis RJ, Letendre SL, Marcotte TD, Atkinson JH, Rivera-Mindt M, Vigil OR, Taylor MJ, Collier AC, Marra CM, Gelman BB, McArthur JC, Morgello S, Simpson DM, McCutchan JA, Abramson I, Gamst A, Fennema-Notestine C, Jernigan TL, Wong J, Grant I; CHARTER Group. HIV-associated neurocognitive disorders persist in the era of potent antiretroviral therapy: CHARTER Study. Neurology. 2010 Dec 7;75(23):2087-96.
65) Hertel J, Struthers H, Horj CB, Hruz PW. A structural basis for the acute effects of HIV protease inhibitors on GLUT4 intrinsic activity. J Biol Chem. 2004 Dec 31;279(53):55147-52.
66) Winocur G, Greenwood C, Pirolli G, Grillo C, Reznikov L, Reagan LP, McEwen BS. Memory impairment in obese zucker rats: An investigation of cognitive function in an animal model of insulin resistance and obesity. Behavioral Neuroscience. 2005;119(5): 1389-1395.
67) Gibbs EM, Stock JL, McCoid SC, Stukenbrok HA, Pessin JE, Stevenson RW, Milici AJ, McNeish JD. Glycemic improvement in diabetic db/db mice by overexpression of the human insulin-regulatable glucose transporter (GLUT4). J Clin Invest. 1995 Apr;95(4):1512-8.
68) Stranahan AM, Arumugam TV, Cutler RG, Lee K, Egan JM, Mattson MP. Diabetes impairs hippocampal function through glucocorticoid-mediated effects on new and mature neurons. Nat Neurosci. 2008 Mar;11(3):309-17.
69) Dey A, Hao S, Wosiski-Kuhn M, Stranahan AM. Glucocorticoid-mediated activation of GSK3β promotes tau phosphorylation and impairs memory in type 2 diabetes. Neurobiol Aging. 2017 Sep;57:75-83.
70) Fujita H, Hatakeyama H, Watanabe TM, Sato M, Higuchi H, Kanzaki M. Identification of three distinct functional sites of insulin-mediated GLUT4 trafficking in adipocytes using quantitative single molecule imaging. Mol Biol Cell. 2010 Aug 1;21(15):2721-31.
71) Hatakeyama H, Kanzaki M. Molecular basis of insulin-responsive GLUT4 trafficking systems revealed by single molecule imaging. Traffic. Volume 12, Issue 12, 2011.
72) Mueckler M. Insulin resistance and the disruption of Glut4 trafficking in skeletal muscle. J Clin Invest. 2001 May;107(10):1211-3.
73) Xu B, English JM, Wilsbacher JL, Stippec S, Goldsmith EJ, Cobb MH. WNK1, a novel mammalian serine/threonine protein kinase lacking the catalytic lysine in subdomain II. J Biol Chem. 2000 Jun 2;275(22):16795-801.
74) Vitari AC, Deak M, Morrice NA, Alessi DR. The WNK1 and WNK4 protein kinases that are mutated in Gordon's hypertension syndrome phosphorylate and activate SPAK and OSR1 protein kinases. Biochem J. 2005 Oct 1;391(Pt 1):17-24.
75) Bercier V, Brustein E, Liao M, Dion PA, Lafrenière RG, Rouleau GA, Drapeau P. WNK1/HSN2

mutation in human peripheral neuropathy deregulates KCC2 expression and posterior lateral line
development in zebrafish (Danio rerio). PLoS Genet. 2013;9(1):e1003124.
76) Piechotta K, Lu J, Delpire E. Cation chloride cotransporters interact with the stress-related kinases
Ste20-related proline-alanine-rich kinase (SPAK) and oxidative stress response 1 (OSR1). J Biol
Chem. 2002;277(52):50812-9.
77) Wang H, Yang J, Schneider JA, De Jager PL, Bennett DA, Zhang HY. Genome-wide interaction analysis of pathological hallmarks in Alzheimer's disease. Neurobiol Aging. 2020 Sep;93:61-68.
78) McClay JL, Adkins DE, Aberg K, Bukszár J, Khachane AN, Keefe RS, Perkins DO, McEvoy JP, Stroup TS, Vann RE, Beardsley PM, Lieberman JA, Sullivan PF, van den Oord EJ. Genome-wide pharmacogenomic study of neurocognition as an indicator of antipsychotic treatment response in schizophrenia. Neuropsychopharmacology. 2011 Feb;36(3):616-26.
79) Stahl EA, Breen G, Forstner AJ, et al. Genome-wide association study identifies 30 loci associated with bipolar disorder. Nat Genet. 2019;51(5):793-803.
80) Lee JJ, Wedow R, Okbay A, et al. Gene discovery and polygenic prediction from a genome-wide association study of educational attainment in 1.1 million individuals. Nat Genet. 2018;50(8):1112-1121. Published 2018 Jul 23.
81) Howard DM, Adams MJ, Clarke TK, et al. Genome-wide meta-analysis of depression identifies 102 independent variants and highlights the importance of the prefrontal brain regions. Nat Neurosci. 2019;22(3):343-352.
82) Baselmans BML, Jansen R, Ip HF, van Dongen J, Abdellaoui A, van de Weijer MP, Bao Y, Smart M, Kumari M, Willemsen G, Hottenga JJ; BIOS consortium; Social Science Genetic Association Consortium, Boomsma DI, de Geus EJC, Nivard MG, Bartels M. Multivariate genome-wide analyses of the well-being spectrum. Nat Genet. 2019 Mar;51(3):445-451.
83) Biernacka JM, Sangkuhl K, Jenkins G, Whaley RM, Barman P, Batzler A, Altman RB, Arolt V, Brockmöller J, Chen CH, Domschke K, Hall-Flavin DK, Hong CJ, Illi A, Ji Y, Kampman O, Kinoshita T, Leinonen E, Liou YJ, Mushiroda T, Nonen S, Skime MK, Wang L, Baune BT, Kato M, Liu YL, Praphanphoj V, Stingl JC, Tsai SJ, Kubo M, Klein TE, Weinshilboum R. The International SSRI Pharmacogenomics Consortium (ISPC): a genome-wide association study of antidepressant treatment response. Transl Psychiatry. 2015 Apr 21; 5(4): e553.
84) International Parkinson Disease Genomics Consortium, Nalls MA, Plagnol V, Hernandez DG, Sharma M, Sheerin UM, Saad M, Simón-Sánchez J, Schulte C, Lesage S, Sveinbjörnsdóttir S, Stefánsson K, Martinez M, Hardy J, Heutink P, Brice A, Gasser T, Singleton AB, Wood NW. Imputation of sequence variants for identification of genetic risks for Parkinson's disease: a meta-analysis of genome-wide association studies. Lancet. 2011 Feb 19;377(9766):641-9.
85) Pickrell, J., Berisa, T., Liu, J. et al. Detection and interpretation of shared genetic influences on 42 human traits. Nat Genet 48, 709–717 (2016).
86) Pankratz N, Beecham GW, DeStefano AL, Dawson TM, Doheny KF, Factor SA, Hamza TH, Hung AY, Hyman BT, Ivinson AJ, Krainc D, Latourelle JC, Clark LN, Marder K, Martin ER, Mayeux R, Ross OA, Scherzer CR, Simon DK, Tanner C, Vance JM,

Wszolek ZK, Zabetian CP, Myers RH, Payami H, Scott WK, Foroud T; PD GWAS Consortium. Meta-analysis of Parkinson's disease: identification of a novel locus, RIT2. Ann Neurol. 2012 Mar; 71(3): 370-84.

87) Nalls MA, Blauwendraat C, Vallerga CL, Heilbron K, Bandres-Ciga S. et al. Identification of novel risk loci, causal insights, and heritable risk for Parkinson's disease: a meta-analysis of genome-wide association studies. Lancet Neurol. 2019 Dec; 18(12): 1091-1102.

88) Nalls MA, Pankratz N, Lill CM, Do CB, Hernandez DG, Saad M, et al. Large-scale meta-analysis of genome-wide association data identifies six new risk loci for Parkinson's disease. Nat Genet. 2014 Sep; 46(9): 989-93.

89) Chang D, Nalls MA, Hallgrímsdóttir IB, Hunkapiller J, van der Brug M, Cai F; International Parkinson's Disease Genomics Consortium; 23andMe Research Team, Kerchner GA, Ayalon G, Bingol B, Sheng M, Hinds D, Behrens TW, Singleton AB, Bhangale TR, Graham RR. A meta-analysis of genome-wide association studies identifies 17 new Parkinson's disease risk loci. Nat Genet. 2017 Oct;49(10):1511-1516.

90) Zhao B, Luo T, Li T, Li Y, Zhang J, Shan Y, Wang X, Yang L, Zhou F, Zhu Z; Alzheimer’s Disease Neuroimaging Initiative; Pediatric Imaging, Neurocognition and Genetics, Zhu H. Genome-wide association analysis of 19,629 individuals identifies variants influencing regional brain volumes and refines their genetic co-architecture with cognitive and mental health traits. Nat Genet. 2019 Nov;51(11):1637-1644.

91) Sherva R, Tripodis Y, Bennett DA, Chibnik LB, Crane PK, de Jager PL, Farrer LA, Saykin AJ, Shulman JM, Naj A, Green RC; GENAROAD Consortium; Alzheimer's Disease Neuroimaging Initiative; Alzheimer's Disease Genetics Consortium. Genome-wide association study of the rate of cognitive decline in Alzheimer's disease. Alzheimers Dement. 2014 Jan;10(1):45-52.

92) Yao X, Glessner JT, Li J, Qi X, Hou X, Zhu C, Li X, March ME, Yang L, Mentch FD, Hain HS, Meng X, Xia Q, Hakonarson H, Li J. Integrative analysis of genome-wide association studies identifies novel loci associated with neuropsychiatric disorders. Transl Psychiatry. 2021 Jan 21;11(1):69.

93) Lee JJ, Wedow R, Okbay A, Kong E, Maghzian O, Zacher M, Nguyen-Viet TA, Bowers P, Sidorenko J, Karlsson Linnér R, Fontana MA, Kundu T, Lee C, Li H, Li R, Royer R, Timshel PN, Walters RK, Willoughby EA, Yengo L; 23andMe Research Team; COGENT (Cognitive Genomics Consortium); Social Science Genetic Association Consortium; Alver M, Bao Y, Clark DW, Day FR, Furlotte NA, Joshi PK, Kemper KE, Kleinman A, Langenberg C, Mägi R, Trampush JW, Verma SS, Wu Y, Lam M, Zhao JH, Zheng Z, Boardman JD, Campbell H, Freese J, Harris KM, Hayward C, Herd P, Kumari M, Lencz T, Luan J, Malhotra AK, Metspalu A, Milani L, Ong KK, Perry JRB, Porteous DJ, Ritchie MD, Smart MC, Smith BH, Tung JY, Wareham NJ, Wilson JF, Beauchamp JP, Conley DC, Esko T, Lehrer SF, Magnusson PKE, Oskarsson S, Pers TH, Robinson MR, Thom K, Watson C, Chabris CF, Meyer MN, Laibson DI, Yang J, Johannesson M, Koellinger PD, Turley P, Visscher PM, Benjamin DJ, Cesarini D. Gene discovery and polygenic prediction from a genome-wide association study of educational attainment in 1.1 million individuals. Nat Genet. 2018 Jul 23;50(8):1112-1121.

94) Küry S, Zhang J, Besnard T, Caro-Llopis A, Zeng X, Robert SM, Josiah SS, Kiziltug E, Denommé-Pichon AS, Cogné B, Kundishora AJ, Hao LT, Li H, Stevenson RE, Louie RJ, Deb W, Torti E, Vignard V, McWalter K, Raymond FL, Rajabi F, Ranza E, Grozeva D, Coury SA, Blanc X, Brischoux-Boucher E, Keren B, Õunap K, Reinson K, Ilves P,

Wentzensen IM, Barr EE, Guihard SH, Charles P, Seaby EG, Monaghan KG, Rio M, van Bever Y, van Slegtenhorst M, Chung WK, Wilson A, Quinquis D, Bréhéret F, Retterer K, Lindenbaum P, Scalais E, Rhodes L, Stouffs K, Pereira EM, Berger SM, Milla SS, Jaykumar AB, Cobb MH, Panchagnula S, Duy PQ, Vincent M, Mercier S, Gilbert-Dussardier B, Le Guillou X, Audebert-Bellanger S, Odent S, Schmitt S, Boisseau P, Bonneau D, Toutain A, Colin E, Pasquier L, Redon R, Bouman A, Rosenfeld JA, Friez MJ, Pérez-Peña H, Akhtar Rizvi SR, Haider S, Antonarakis SE, Schwartz CE, Martínez F, Bézieau S, Kahle KT, Isidor B. Rare pathogenic variants in WNK3 cause X-linked intellectual disability. Genet Med. 2022 Sep;24(9):1941-1951.

95) Ray M, Zhang W. Analysis of Alzheimer's disease severity across brain regions by topological analysis of gene co-expression networks. BMC Syst Biol. 2010; 4: 136.

96) Kumar P, Dezso Z, MacKenzie C, et al. Circulating miRNA biomarkers for Alzheimer's disease. PLoS One. 2013; 8(7): e69807.

97) Qin Y, Wang G, Peng Z. MicroRNA-191-5p diminished sepsis-induced acute kidney injury through targeting oxidative stress responsive 1 in rat models. Biosci Rep. 2019; 39(8): BSR20190548.

98) Faisal FE, Milenković T. Dynamic networks reveal key players in aging. Bioinformatics. 2014 Jun 15;30(12):1721-9.

99) Arion D, Lewis DA. Altered expression of regulators of the cortical chloride transporters NKCC1 and KCC2 in schizophrenia. Arch Gen Psychiatry. 2011 Jan;68(1):21-31.

100) Shekarabi M, Girard N, Rivière JB, et al. Mutations in the nervous system--specific HSN2 exon of WNK1 cause hereditary sensory neuropathy type II. J Clin Invest. 2008; 118(7): 2496-2505.

101) Puthiyedth N, Riveros C, Berretta R, Moscato P. Identification of Differentially Expressed Genes through Integrated Study of Alzheimer's Disease Affected Brain Regions. PLoS One. 2016; 11(4): e0152342.

102) Fernandez-Enright F, Andrews JL, Newell KA, Pantelis C, Huang XF. Novel implications of Lingo-1 and its signaling partners in schizophrenia. Transl Psychiatry. 2014 Jan 21;4(1):e348.

103) Moore YE, Conway LC, Wobst HJ, Brandon NJ, Deeb TZ, Moss SJ. Developmental Regulation of KCC2 Phosphorylation Has Long-Term Impacts on Cognitive Function. Front Mol Neurosci. 2019 Jul 23;12:173.

104) Friedel P, Kahle KT, Zhang J, Hertz N, Pisella LI, Buhler E, et al. WNK1-regulated inhibitory phosphorylation of the KCC2 cotransporter maintains the depolarizing action of GABA in immature neurons. Sci Signal. 2015; 8(383): ra65–ra.

105) Goutierre M, Al Awabdh S, Donneger F, François E, Gomez-Dominguez D, Irinopoulou T, Menendez de la Prida L, Poncer JC. KCC2 Regulates Neuronal Excitability and Hippocampal Activity via Interaction with Task-3 Channels. Cell Rep. 2019 Jul 2;28(1):91-103.e7.

106) Merner ND, Chandler MR, Bourassa C, Liang B, Khanna AR, Dion P, et al. Regulatory domain or CpG site variation in SLC12A5, encoding the chloride transporter KCC2, in human autism and schizophrenia. Frontiers in cellular neuroscience. 2015; 9.

107) Lee AY, Chen W, Stippec S, et al. Protein kinase WNK3 regulates the neuronal splicing factor Fox-1. PNAS. 2012; 109(42): 16841-16846.

108) Begum G, Yuan H, Kahle KT, Li L, Wang S, Shi Y, Shmukler BE, Yang SS, Lin SH, Alper SL, Sun D. Inhibition of WNK3 Kinase Signaling Reduces Brain Damage and Accelerates Neurological Recovery After Stroke. Stroke. 2015 Jul;46(7):1956-1965.

109) Jeong KH, Kim SH, Choi YH, Cho I, Kim WJ. Increased expression of WNK3 in dispersed granule cells in hippocampal sclerosis of mesial temporal lobe epilepsy patients. Epilepsy Res. 2018 Nov; 147: 58-61.
110) Taylor CA 4th, An SW, Kankanamalage SG, Stippec S, Earnest S, Trivedi AT, Yang JZ, Mirzaei H, Huang CL, Cobb MH. OSR1 regulates a subset of inward rectifier potassium channels via a binding motif variant. Proc Natl Acad Sci U S A. 2018 Apr 10;115(15):3840-3845.
111) Zhou B, Zhuang J, Gu D, Wang H, Cebotaru L, Guggino WB, Cai H. WNK4 enhances the degradation of NCC through a sortilin-mediated lysosomal pathway. J Am Soc Nephrol. 21: 82–92.
112) Shekarabi M, Zhang J, Khanna AR, Ellison DH, Delpire E, Kahle KT. WNK Kinase Signaling in Ion Homeostasis and Human Disease. Cell Metab. 2017 Feb 7;25(2):285-299.
113) Moriguchi T, Urushiyama S, Hisamoto N, Iemura SI, Uchida S, Natsume T, Matsumoto K, Shibuya H. WNK1 regulates phosphorylation of cation-chloride-coupled cotransporters via the STE20-related kinases, SPAK and OSR1. J Biol Chem. 2005; 280: 42685–42693.
114) Lee BH, Min X, Heise CJ, Xu BE, Chen S, Shu H, Luby-Phelps K, Goldsmith EJ, Cobb MH. WNK1 phosphorylates synaptotagmin 2 and modulates its membrane binding. Mol Cell. 2004 Sep 10;15(5):741-51.
115) Oh E, Heise CJ, English JM, Cobb MH, Thurmond DC. WNK1 is a novel regulator of Munc18c-syntaxin 4 complex formation in soluble NSF attachment protein receptor (SNARE)-mediated vesicle exocytosis. J Biol Chem. 2007;282(45):32613-22.
116) Mendes AI, Matos P, Moniz S, Jordan P. Protein kinase WNK1 promotes cell surface expression of glucose transporter GLUT1 by regulating a Tre-2/USP6-BUB2-Cdc16 domain family member 4 (TBC1D4)-Rab8A complex. J Biol Chem. 2010 Dec 10; 285(50): 39117-26.
117) Henriques AFA, Matos P, Carvalho AS, Azkargorta M, Elortza F, Matthiesen R, Jordan P. WNK1 phosphorylation sites in TBC1D1 and TBC1D4 modulate cell surface expression of GLUT1. Arch Biochem Biophys. 2020; 679: 108223.
118) Sakamoto K, Holman GD. Emerging role for AS160/TBC1D4 and TBC1D1 in the regulation of GLUT4 traffic. Am J Physiol Endocrinol Metab. 2008; 295(1): E29-E37.
119) Kim JH, Kim H, Hwang KH, Chang JS, Park KS, Cha SK, Kong ID. WNK1 kinase is essential for insulin-stimulated GLUT4 trafficking in skeletal muscle. FEBS Open Bio. 2018;8(11):1866-1874.
120) Ellison DH, Oyama TT, Yang CL, Rogers S, Beard DR, Komers R. Altered WNK4/NCC signaling in a rat model of insulin resistance. J AM Soc Nephrol 20: 100A, 2009
121) Komers R, Rogers S, Oyama TT, Xu B, Yang CL, McCormick J, Ellison DH. Enhanced phosphorylation of Na(+)-Cl- co-transporter in experimental metabolic syndrome: role of insulin. Clin Sci (Lond). 2012 Dec;123(11):635-47.
122) Nishida H, Sohara E, Nomura N, Chiga M, Alessi DR, Rai T, Sasaki S, Uchida S. Phosphatidylinositol 3-kinase/Akt signaling pathway activates the WNK-OSR1/SPAK-NCC phosphorylation cascade in hyperinsulinemic db/db mice. Hypertension. 2012 Oct;60(4):981-90.
123) Sohara E, Rai T, Yang SS, Ohta A, Naito S, Chiga M, Nomura N, Lin SH, Vandewalle A, Ohta E, Sasaki S, Uchida S. Acute insulin stimulation induces phosphorylation of the

Na-Cl cotransporter in cultured distal mpkDCT cells and mouse kidney. PLoS One. 2011; 6:e24277.
124) Jiang ZY, Zhou QL, Holik J, Patel S, Leszyk J, Coleman K, Chouinard M, Czech MP. Identification of WNK1 as a substrate of Akt/protein kinase B and a negative regulator of insulin-stimulated mitogenesis in 3T3-L1 cells. J Biol Chem. 2005 Jun 3;280(22):21622-8.
125) Vitari AC, Deak M, Collins BJ, Morrice N, Prescott AR, Phelan A, Humphreys S, Alessi DR. WNK1, the kinase mutated in an inherited high-blood-pressure syndrome, is a novel PKB (protein kinase B)/Akt substrate. Biochem J. 2004; 378(Pt 1): 257-68.
126) Yoshizaki Y, Mori Y, Tsuzaki Y, Mori T, Nomura N, Wakabayashi M, Takahashi D, Zeniya M, Kikuchi E, Araki Y, Ando F, Isobe K, Nishida H, Ohta A, Susa K, Inoue Y, Chiga M, Rai T, Sasaki S, Uchida S, Sohara E. Impaired degradation of WNK by Akt and PKA phosphorylation of KLHL3. Biochem Biophys Res Commun. 2015 Nov 13;467(2):229-34.
127) Xu BE, Stippec S, Lazrak A, Huang CL, Cobb MH. WNK1 activates SGK1 by a phosphatidylinositol 3-kinase-dependent and non-catalytic mechanism. J Biol Chem. 2005; 280(40):34218–23.
128) Cheng CJ, Huang CL. Activation of PI3-kinase stimulates endocytosis of ROMK via Akt1/SGK1-dependent phosphorylation of WNK1. J Am Soc Nephrol. 2011;22(3):460–71
129) Ding L, Zhang L, Biswas S, Schugar RC, Brown JM, Byzova T, Podrez E. Akt3 inhibits adipogenesis and protects from diet-induced obesity via WNK1/SGK1 signaling. JCI Insight. 2017 Nov 16;2(22):e95687.
130) Takahashi D, Mori T, Sohara E, Tanaka M, Chiga M, Inoue Y, Nomura N, Zeniya M, Ochi H, Takeda S, Suganami T, Rai T, Uchida S. WNK4 is an Adipogenic Factor and Its Deletion Reduces Diet-Induced Obesity in Mice. EBioMedicine. 2017 Apr;18:118-127.
131) Yamada K, Park HM, Rigel DF, DiPetrillo K, Whalen EJ, Anisowicz A, Beil M, Berstler J, Brocklehurst CE, Burdick DA, Caplan SL, Capparelli MP, Chen G, Chen W, Dale B, Deng L, Fu F, Hamamatsu N, Harasaki K, Herr T, Hoffmann P, Hu QY, Huang WJ, Idamakanti N, Imase H, Iwaki Y, Jain M, Jeyaseelan J, Kato M, Kaushik VK, Kohls D, Kunjathoor V, LaSala D, Lee J, Liu J, Luo Y, Ma F, Mo R, Mowbray S, Mogi M, Ossola F, Pandey P, Patel SJ, Raghavan S, Salem B, Shanado YH, Trakshel GM, Turner G, Wakai H, Wang C, Weldon S, Wielicki JB, Xie X, Xu L, Yagi YI, Yasoshima K, Yin J, Yowe D, Zhang JH, Zheng G, Monovich L. Small-molecule WNK inhibition regulates cardiovascular and renal function. Nat Chem Biol. 2016 Nov;12(11):896-898.
132) Kovalevich J, Langford D. Considerations for the use of SH-SY5Y neuroblastoma cells in neurobiology. Methods Mol Biol. 2013;1078:9-21.
133) Villa F, Goebel J, Rafiqi FH, et al. Structural insights into the recognition of substrates and activators by the OSR1 kinase. EMBO Rep. 2007; 8(9): 839-845.
134) Clinton A Taylor IV, Ji-Ung Jung, Sachith Gallolu Kankanamalage, Justin Li, Magdalena Grzemska,
Ankita B. Jaykumar, Svetlana Earnest, Steve Stippec, Purbita Saha, Eustolia Sauceda, Melanie H.
Cobb. Motif Recognition by Signaling Partners of the Kinases OSR1 and SPAK Identify More Targets
of the WNK Pathway. (Soon to be submitted).

135) Shi J, Kandror KV. Sortilin is essential and sufficient for the formation of Glut4 storage vesicles in 3T3-L1 adipocytes. Dev Cell 2005; 9:99–108.
136) Pan X, Zaarur N, Singh M, Morin P, Kandror KV. Sortilin and retromer mediate retrograde transport of Glut4 in 3T3-L1 adipocytes. Mol Biol Cell. 2017; 28(12): 1667-1675.
137) Lin BZ, Pilch PF, Kandror KV. Sortilin is a major protein component of Glut4-containing vesicles. J Biol Chem 1997;272:24145–24147.
138) Huang G, Buckler-Pena D, Nauta T, Singh M, Asmar A, Shi J, Kim JY, Kandror KV. Insulin responsiveness of glucose transporter 4 in 3T3-L1 cells depends on the presence of sortilin. Mol Biol Cell. 2013;24(19):3115-22.
139) Ariga M, Nedachi T, Katagiri H, Kanzaki M. Functional role of sortilin in myogenesis and development of insulin-responsive glucose transport system in C2C12 myocytes.J Biol Chem. 2008; 283:10208–10220
140) Seaman MN. Identification of a novel conserved sorting motif required for retromer-mediated endosome-to-TGN retrieval. J Cell Sci. 2007;120(Pt 14):2378-89.
141) Nielsen MS, Madsen P, Christensen EI, et al. The sortilin cytoplasmic tail conveys Golgi-endosome transport and binds the VHS domain of the GGA2 sorting protein. EMBO J. 2001;20(9):2180-2190.
142) Zaarur N, Meriin AB, Singh M, Goel RK, Zaia J, Kandror KV. Akt may associate with insulin-responsive vesicles via interaction with sortilin. FEBS Lett. 2024 Feb;598(4):390-399.
143) Fu X, Zhang Y, Zhang R. Regulatory role of PI3K/Akt/WNK1 signal pathway in mouse model of bone cancer pain. Sci Rep. 2023 Aug 31;13(1):14321.
144) Zheng H, Zheng Y, Zhao L, Chen M, Bai G, Hu Y, Hu W, Yan Z, Gao H. Cognitive decline in type 2 diabetic db/db mice may be associated with brain region-specific metabolic disorders. Biochim Biophys Acta Mol Basis Dis. 2017 Jan;1863(1):266-273.
145) Ramos-Rodriguez JJ, Ortiz O, Jimenez-Palomares M, Kay KR, Berrocoso E, Murillo-Carretero MI, Perdomo G, Spires-Jones T, Cozar-Castellano I, Lechuga-Sancho AM, Garcia-Alloza M. Differential central pathology and cognitive impairment in pre-diabetic and diabetic mice. Psychoneuroendocrinology. 2013 Nov;38(11):2462-75.
146) Tomassoni D, Martinelli I, Moruzzi M, Micioni Di Bonaventura MV, Cifani C, Amenta F, Tayebati SK. Obesity and Age-Related Changes in the Brain of the Zucker Leprfa/fa Rats. Nutrients. 2020 May 9; 12(5): 1356.
147) Špolcová A, Mikulášková B, Kršková K, Gajdošechová L, Zórad Š, Olszanecki R, Suski M, Bujak-Giżycka B, Železná B, Maletínská L. Deficient hippocampal insulin signaling and augmented Tau phosphorylation is related to obesity- and age-induced peripheral insulin resistance: a study in Zucker rats. BMC Neurosci. 2014 Sep 25; 15: 111.
148) Carvalheira JBC, Ribeiro EB, Araújo EP. et al. Selective impairment of insulin signalling in the hypothalamus of obese Zucker rats. Diabetologia 46, 1629–1640 (2003).
149) Hooper C, Killick R, Lovestone S. The GSK3 hypothesis of Alzheimer's disease. J Neurochem. 2008 Mar;104(6):1433-9.
150) Shao J, Yamashita H, Qiao L, Friedman JE. Decreased Akt kinase activity and insulin resistance in C57BL/KsJ-Leprdb/db mice. J Endocrinol. 2000 Oct;167(1):107-15.
151) Dey A, Hao S, Wosiski-Kuhn M, Stranahan AM. Glucocorticoid-mediated activation of GSK3β promotes tau phosphorylation and impairs memory in type 2 diabetes. Neurobiol Aging. 2017 Sep;57:75-83.

152) Howell KR, Floyd K, Law AJ. PKBγ/AKT3 loss-of-function causes learning and memory deficits and deregulation of AKT/mTORC2 signaling: Relevance for schizophrenia. PLoS One. 2017 May 3;12(5):e0175993.
153) Wong H, Levenga J, LaPlante L, Keller B, Cooper-Sansone A, Borski C, Milstead R, Ehringer M, Hoeffer C. Isoform-specific roles for AKT in affective behavior, spatial memory, and extinction related to psychiatric disorders. Elife. 2020 Dec 16;9:e56630.
154) Dumon C, Diabira D, Chudotvorova I, et al. The adipocyte hormone leptin sets the emergence of hippocampal inhibition in mice. Elife. 2018;7:e36726. Published 2018 Aug 14.
155) Ma DL, Chen FQ, Xu WJ, Yue WZ, Yuan G, Yang Y. Early intervention with glucagon-like peptide 1 analog liraglutide prevents tau hyperphosphorylation in diabetic db/db mice. J Neurochem. 2015 Oct;135(2):301-8.
156) Yi JH, Baek SJ, Heo S, Park HJ, Kwon H, Lee S, Jung J, Park SJ, Kim BC, Lee YC, Ryu JH, Kim DH. Direct pharmacological Akt activation rescues Alzheimer's disease like memory impairments and aberrant synaptic plasticity. Neuropharmacology. 2018 Jan;128:282-292.
157) Nykjaer A, Willnow TE. Sortilin: a receptor to regulate neuronal viability and function. Trends Neurosci. 2012 Apr;35(4):261-70.
158) Chen ZY, Ieraci A, Teng H, Dall H, Meng CX, Herrera DG, Nykjaer A, Hempstead BL, Lee FS. Sortilin controls intracellular sorting of brain-derived neurotrophic factor to the regulated secretory pathway. J Neurosci. 2005 Jun 29;25(26):6156-66.
159) Carlo AS, Gustafsen C, Mastrobuoni G, Nielsen MS, Burgert T, Hartl D, Rohe M, Nykjaer A, Herz J, Heeren J, Kempa S, Petersen CM, Willnow TE. The pro-neurotrophin receptor sortilin is a major neuronal apolipoprotein E receptor for catabolism of amyloid-β peptide in the brain. J Neurosci. 2013 Jan 2;33(1):358-70.
160) Andersson CH, Hansson O, Minthon L, et al. A Genetic Variant of the Sortilin 1 Gene is Associated with Reduced Risk of Alzheimer's Disease. J Alzheimers Dis. 2016;53(4):1353-1363.
161) Lambert JC et al. Meta-analysis of 74,046 individuals identifies 11 new susceptibility loci for Alzheimer’s disease. Nat Genet. Nat Genet. 2013 Dec;45(12):1452-8.
162) Rogaeva E, Meng Y, Lee JH, Gu Y, Kawarai T, Zou F, Katayama T, Baldwin CT, Cheng R, Hasegawa H, Chen F, Shibata N, Lunetta KL, Pardossi-Piquard R, Bohm C, Wakutani Y, Cupples LA, Cuenco KT, Green RC, Pinessi L, Rainero I, Sorbi S, Bruni A, Duara R, Friedland RP, Inzelberg R, Hampe W, Bujo H, Song YQ, Andersen OM, Willnow TE, Graff-Radford N, Petersen RC, Dickson D, Der SD, Fraser PE, Schmitt-Ulms G, Younkin S, Mayeux R, Farrer LA, St George-Hyslop P. The neuronal sortilin-related receptor SORL1 is genetically associated with Alzheimer disease. Nat Genet. 2007 Feb;39(2):168-77.
163) Kunkle BW et al. Genetic meta-analysis of diagnosed Alzheimer’s disease identifies new risk loci and implicates Aβ, tau, immunity and lipid processing. Nat Genet. 2019 Mar;51(3):414-430.
164) Reynolds CA, Zavala C, Gatz M, Vie L, Johansson B, Malmberg B, Ingelsson E, Prince JA, Pedersen NL. Sortilin receptor 1 predicts longitudinal cognitive change. Neurobiol Aging. 2013;34(6):1710.
165) Corder EH, Saunders AM, Strittmatter WJ, et al. Gene dose of apolipoprotein E type 4 allele and the risk of Alzheimer's disease in late onset families. Science. 1993;261:921-923.

166) Holtzman DM, Bales KR, Tenkova T, et al. Apolipoprotein E isoform-dependent amyloid deposition and neuritic degeneration in a mouse model of Alzheimer's disease. PNAS. 2000; 97(6): 2892-2897.
167) Liu CC, Zhao N, Fu Y, Wang N, Linares C, Tsai CW, Bu G. ApoE4 Accelerates Early Seeding of Amyloid Pathology. Neuron. 2017;96(5):1024-1032.e3.
168) Bretsky PM, Buckwalter JG, Seeman TE, Miller CA, Poirier J, Schellenberg GD, Finch CE, Henderson VW. Evidence for an interaction between apolipoprotein E genotype, gender, and Alzheimer disease. Alzheimer Dis Assoc Disord. 1999 Oct-Dec;13(4):216-21.
169) Zhao N, Liu CC, Van Ingelgom AJ, Martens YA, Linares C, Knight JA, Painter MM, Sullivan PM, Bu G. Apolipoprotein E4 Impairs Neuronal Insulin Signaling by Trapping Insulin Receptor in the Endosomes. Neuron. 2017 Sep 27;96(1):115-129.e5.
170) Keeney JT, Ibrahimi S, Zhao L. Human ApoE Isoforms Differentially Modulate Glucose and Amyloid Metabolic Pathways in Female Brain: Evidence of the Mechanism of Neuroprotection by ApoE2 and Implications for Alzheimer's Disease Prevention and Early Intervention. J Alzheimers Dis. 2015;48(2):411-24.
171) Shekarabi M, Lafrenière RG, Gaudet R, Laganière J, Marcinkiewicz MM, Dion PA, Rouleau GA. Comparative analysis of the expression profile of Wnk1 and Wnk1/Hsn2 splice variants in developing and adult mouse tissues. PLoS One. 2013;8(2):e57807.
172) Piton A, Gauthier J, Hamdan FF, Lafrenière RG, Yang Y, Henrion E, Laurent S, Noreau A, Thibodeau P, Karemera L, Spiegelman D, Kuku F, Duguay J, Destroismaisons L, Jolivet P, Côté M, Lachapelle K, Diallo O, Raymond A, Marineau C, Champagne N, Xiong L, Gaspar C, Rivière JB, Tarabeux J, Cossette P, Krebs MO, Rapoport JL, Addington A, Delisi LE, Mottron L, Joober R, Fombonne E, Drapeau P, Rouleau GA. Systematic resequencing of X-chromosome synaptic genes in autism spectrum disorder and schizophrenia. Mol Psychiatry. 2011 Aug;16(8):867-80.
173) Kong LL, Miao D, Tan L, Liu SL, Li JQ, Cao XP, Tan L; Alzheimer’s Disease Neuroimaging Initiative*. Genome-wide association study identifies RBFOX1 locus influencing brain glucose metabolism. Ann Transl Med. 2018 Nov;6(22):436.
174) Ryan AS. Insulin resistance with aging: effects of diet and exercise. Sports Med. 2000 Nov;30(5):327-46.
175) American Diabetes Association. 12. Older Adults: Standards of Medical Care in Diabetes-2020. Diabetes Care. 2020 Jan;43(Suppl 1):S152-S162.
176) Pfeiffer BE, Huber KM. Fragile X mental retardation protein induces synapse loss through acute postsynaptic translational regulation. J Neurosci. 2007 Mar 21;27(12):3120-30.
177) Nosyreva ED, Huber KM. Developmental switch in synaptic mechanisms of hippocampal metabotropic glutamate receptor-dependent long-term depression. J Neurosci. 2005 Mar 16;25(11):2992-3001.
178) Bumeister R, Rosse C, Anselmo A, Camonis J, White MA. CNK2 couples NGF signal propagation to multiple regulatory cascades driving cell differentiation. Curr Biol. 2004 Mar 9;14(5):439-45.
179) Jaykumar AB, Caceres PS, King-Medina KN, Liao TD, Datta I, Maskey D, Naggert JK, Mendez M, Beierwaltes WH, Ortiz PA. Role of Alström syndrome 1 in the regulation of blood pressure and renal function. JCI Insight. 2018 Nov 2;3(21):e95076.

180) Barylko B, Wilkerson JR, Cavalier SH, Binns DD, James NG, Jameson DM, Huber KM, Albanesi JP. Palmitoylation and Membrane Binding of Arc/Arg3.1: A Potential Role in Synaptic Depression. Biochemistry. 2018 Feb 6;57(5):520-524.

Main Figures

Figure1: Inhibition of hippocampal WNK in mice enhances learning and memory

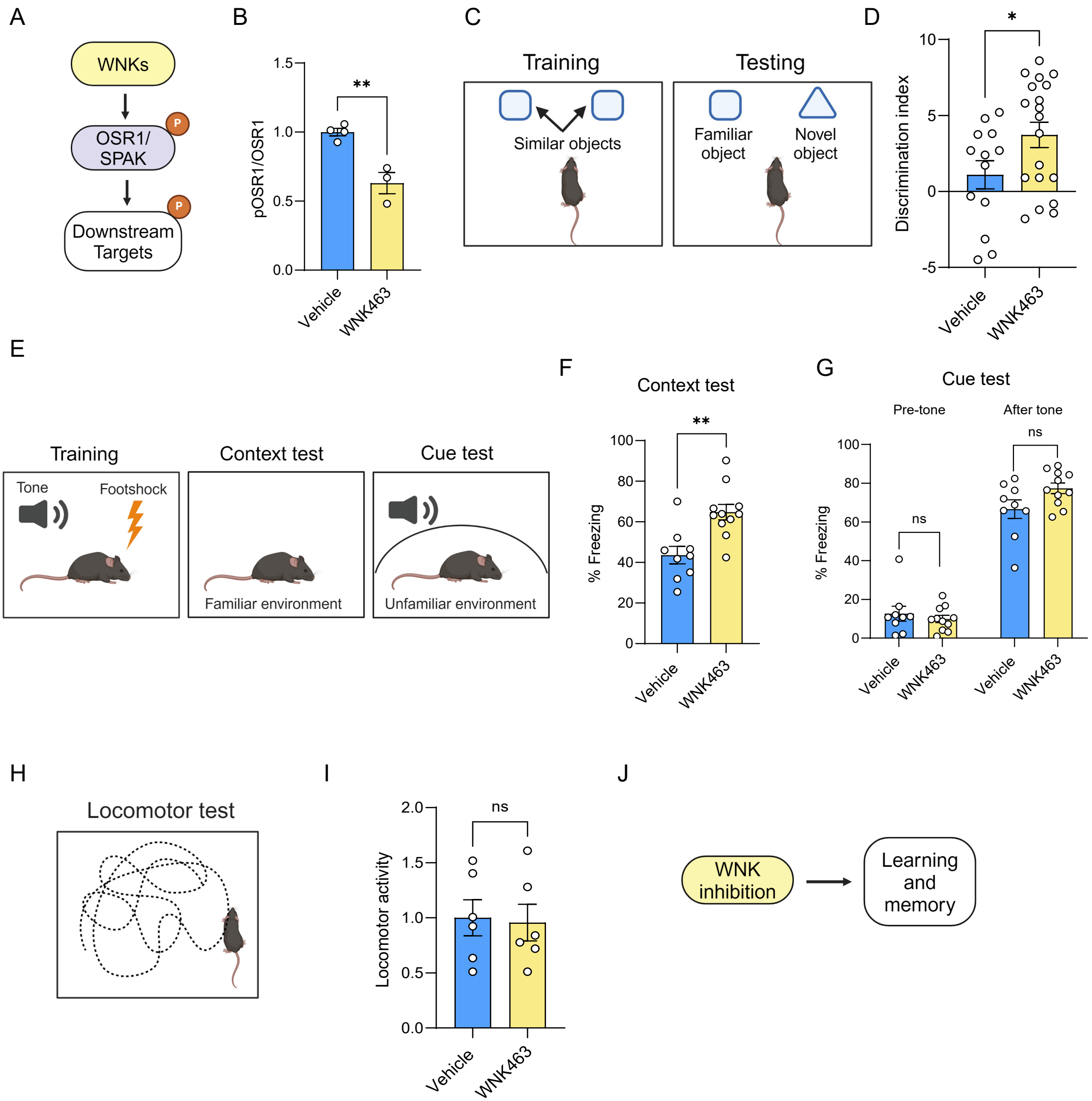

Figure 2: Inhibition of hippocampal WNK enhances anxiety-related behavior in mice

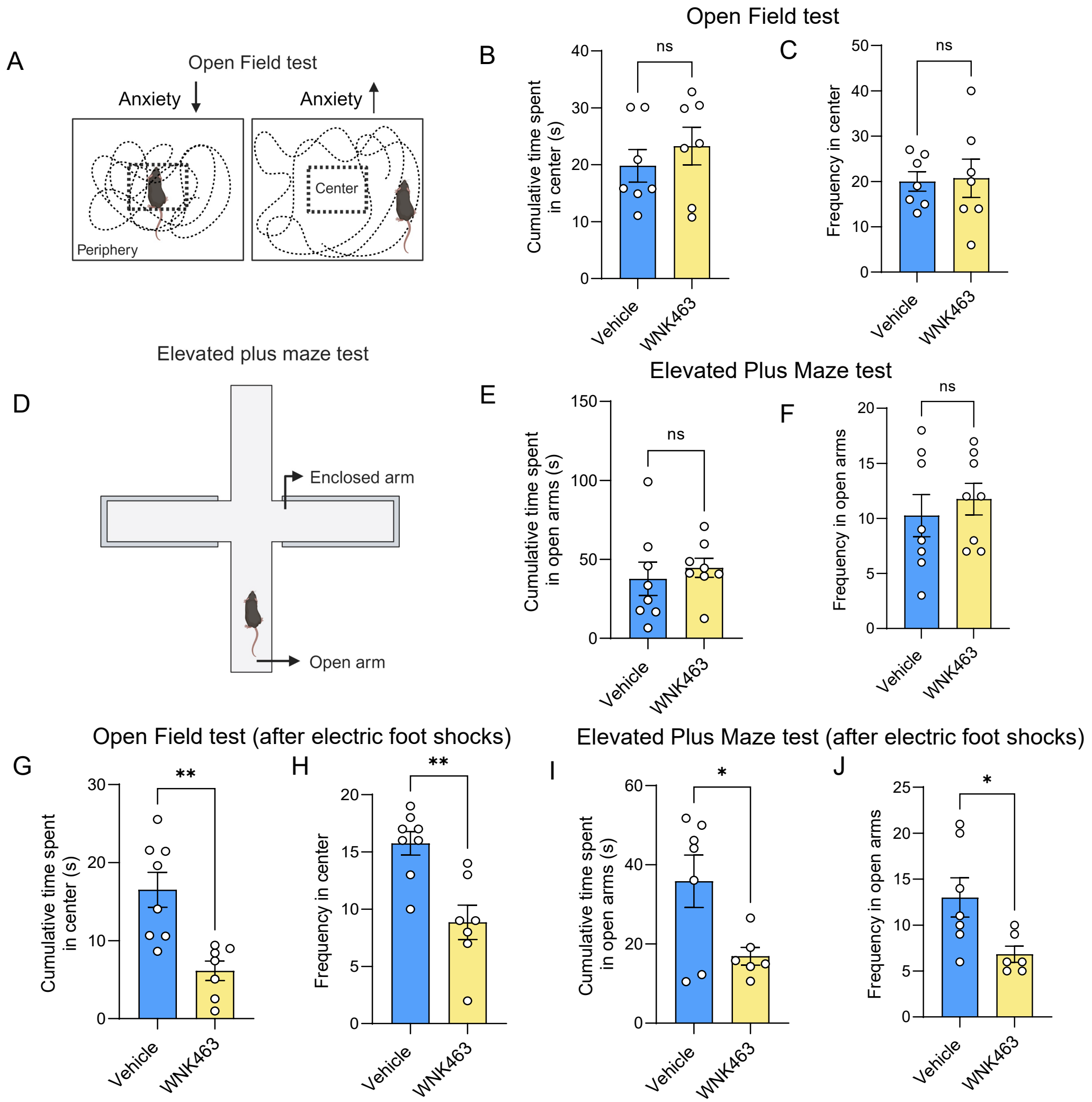

Figure 3: Inhibition of WNK augments glucose uptake via GLUT4

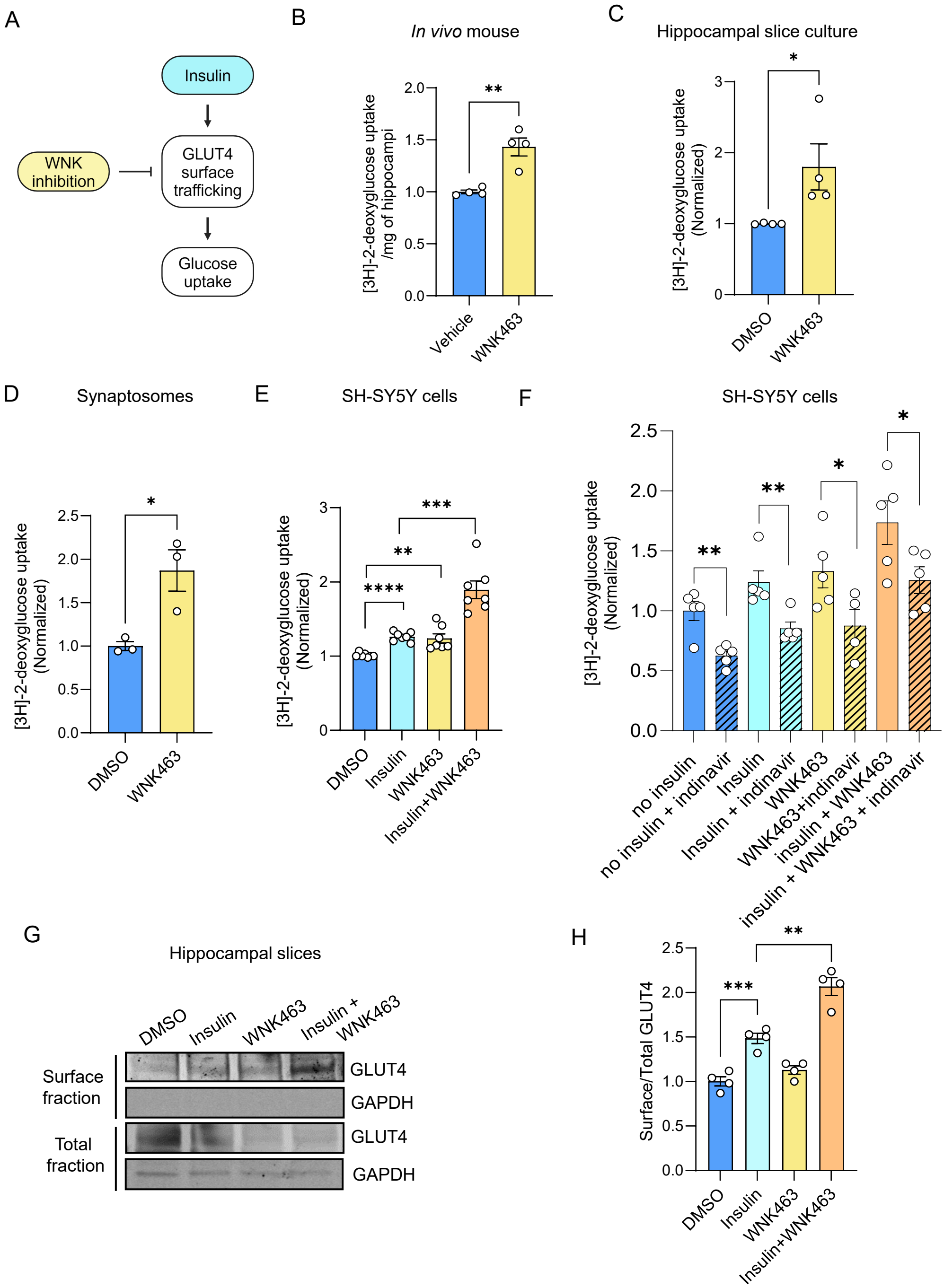

Figure 4: Inhibition of WNK enhances AKT signaling in the hippocampus and cell culture

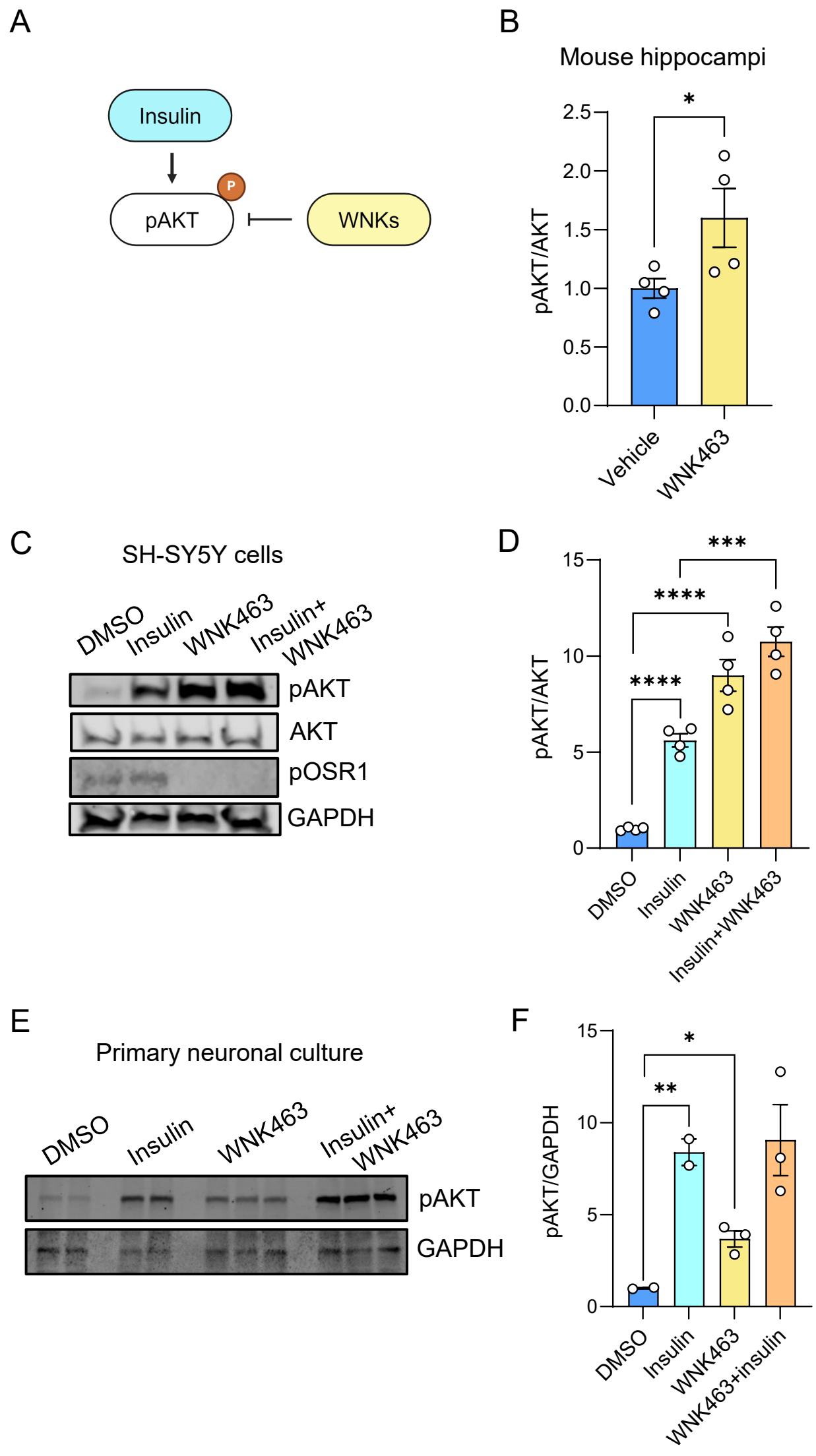

Figure 5: OSR1 interacts with molecular mediators involved in GLUT4 trafficking

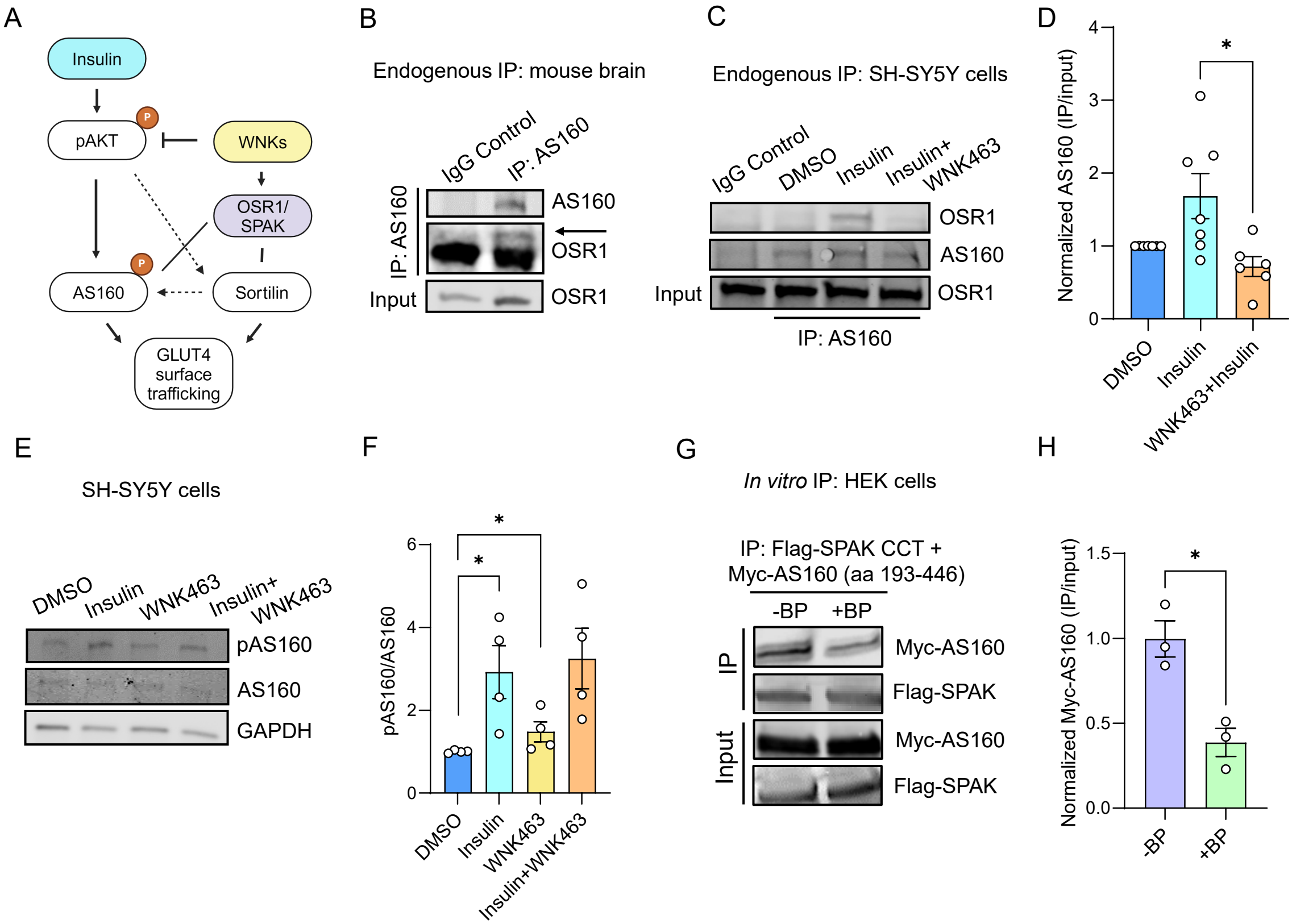

I

SH-SY5Y cells

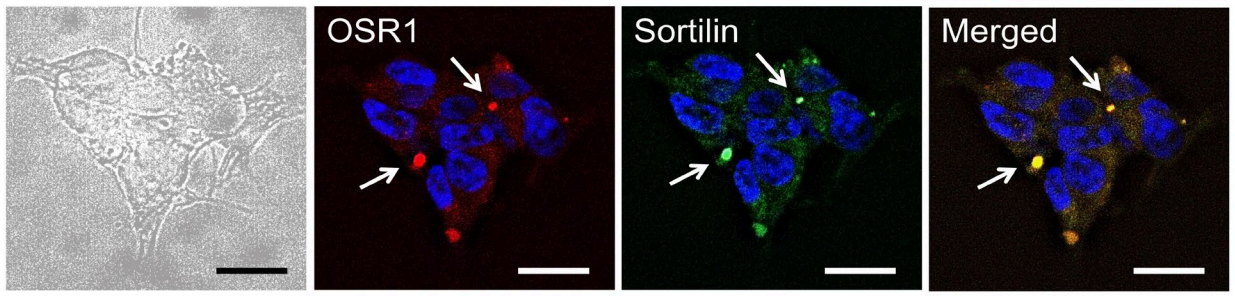

J

Endogenous IP: SH-SY5Y cells

K

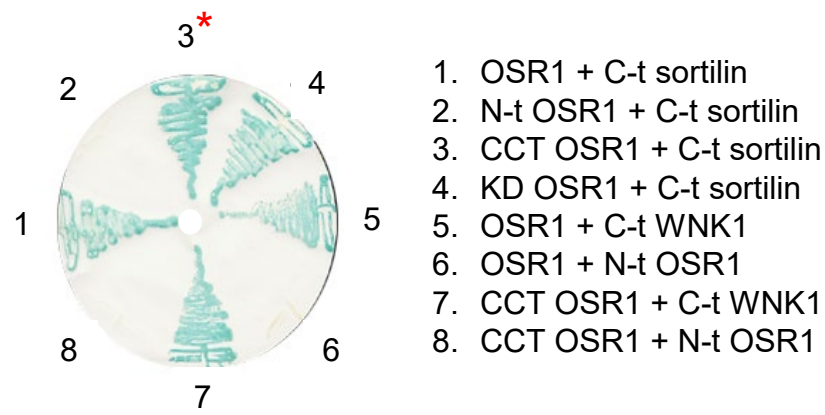

L

HEK cells

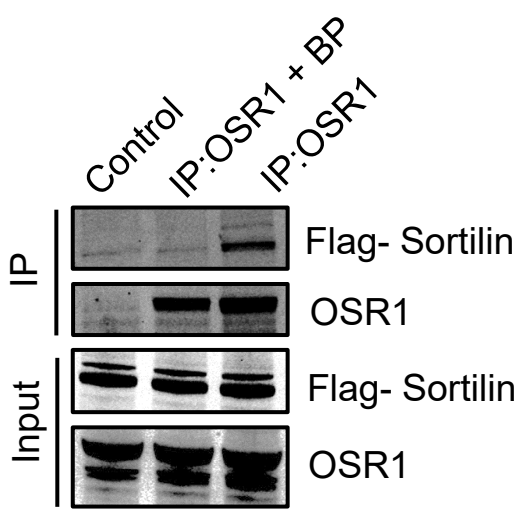

M

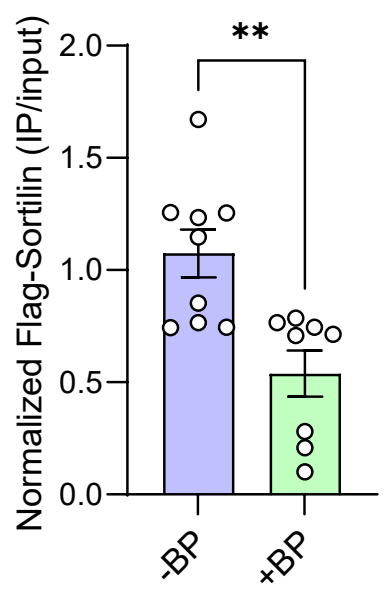

Supplementary Figures

S1A

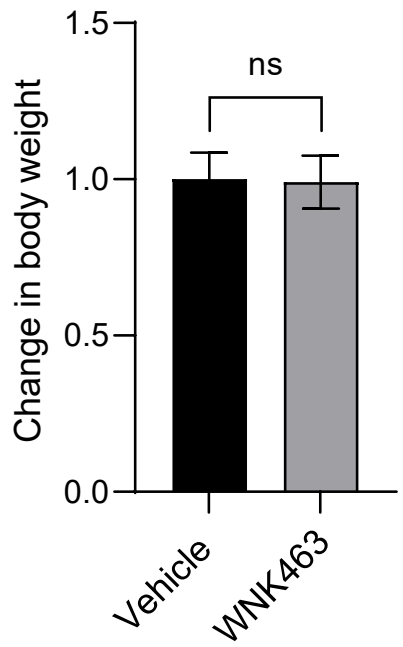

S2A

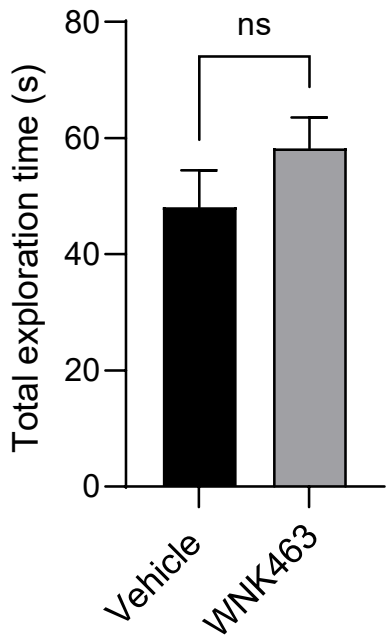

S3A

OFT before electric foot shock

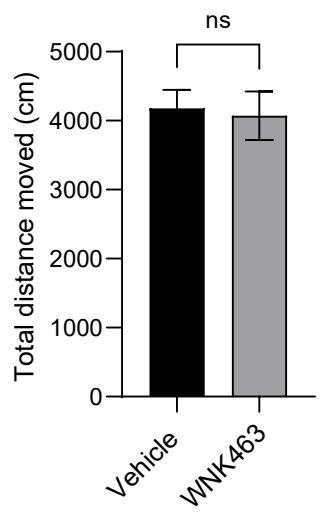

S3B

OFT after electric foot shock

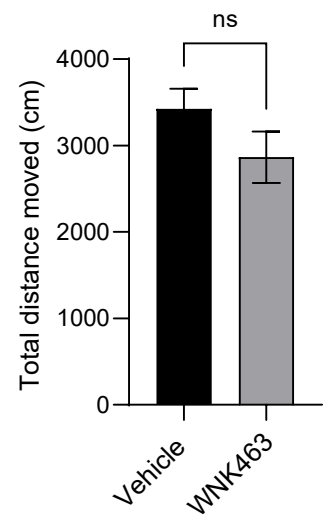

S3C

EPM before electric foot shock

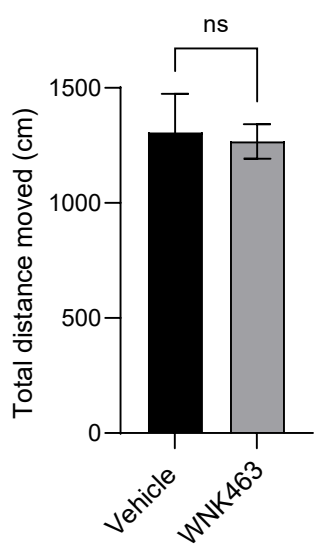

S3D

EPM after electric foot shock

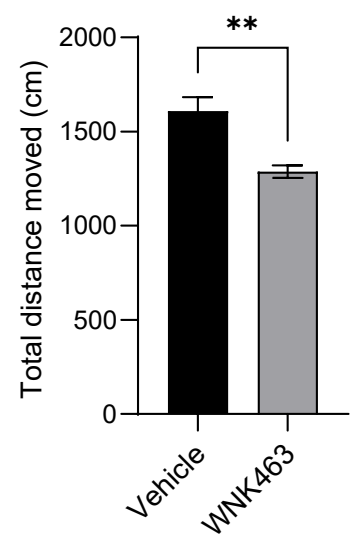

S4A

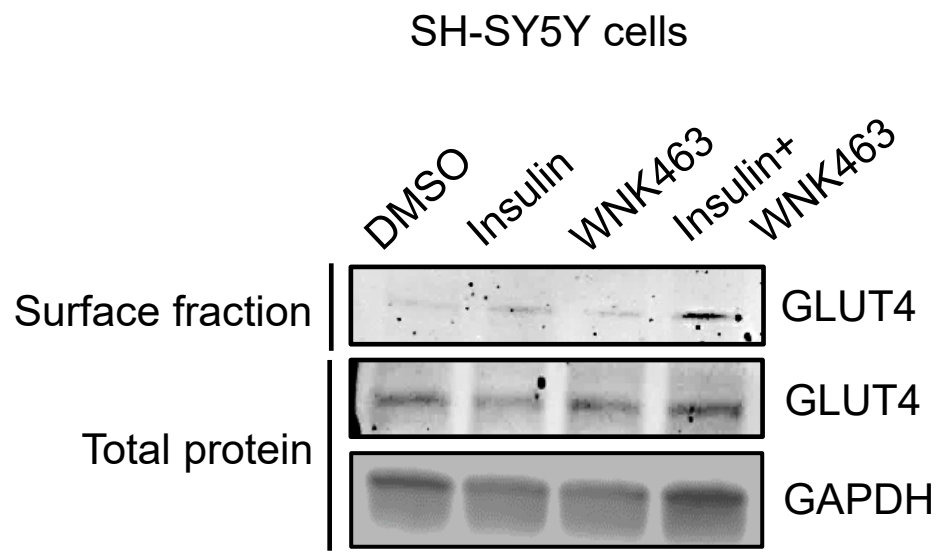
SH-SY5Y cells
DMSO
Insulin
WNK463
Insulin+
WNK463
Surface fraction
GLUT4
Total protein
GLUT4
GAPDH

S4B

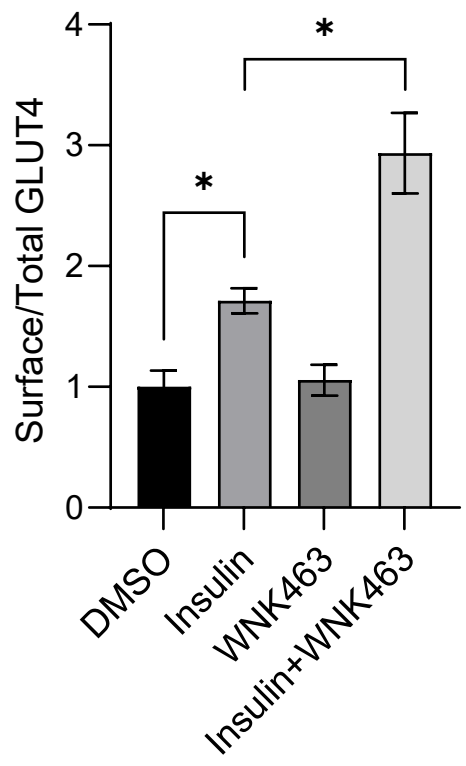
Surface/Total GLUT4
0
1
2
3
4
*
*
DMSO
Insulin
WNK463
Insulin+WNK463

S5A

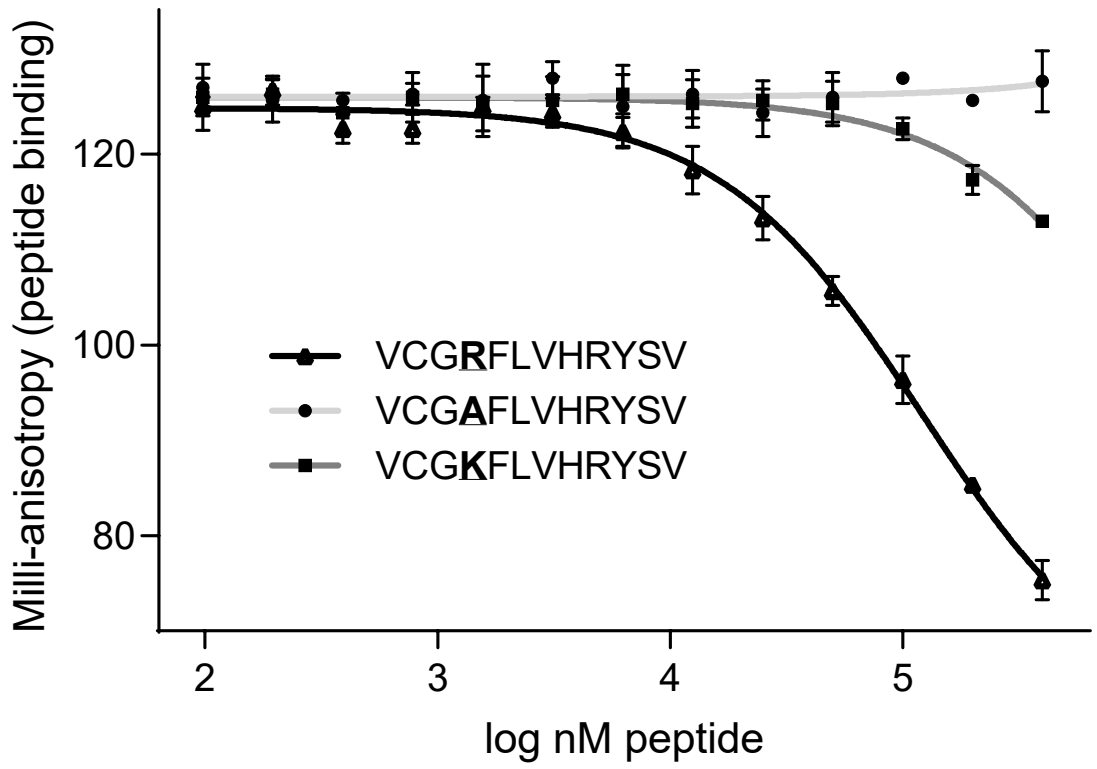
Milli-anisotropy (peptide binding)
120
100
80
2
3
4
5
log nM peptide
VCGRFLVHRYSV
VCGAFLVHRYSV
VCGKFLVHRYSV